Monthly Notices of the ROYAL ASTRONOMICAL SOCIETY

MNRAS **448,** 1118–1136 (2015) doi:10.1093/mnras/stu2728

The HU Aqr planetary system hypothesis revisited

K. Goździewski,[1★] A. Słowikowska,[2] D. Dimitrov,[3] K. Krzeszowski,[2] M. Żejmo,[2] G. Kanbach,[4] V. Burwitz,[4] A. Rau,[4] P. Irawati,[5] A. Richichi,[5] M. Gawroński,[1] G. Nowak,[1,6,7] I. Nasiroglu[8] and D. Kubicki[1]

[1]*Toruń Centre for Astronomy, Faculty of Physics, Astronomy and Applied Informatics, N. Copernicus University, Grudziadzka 5, PL-87-100 Toruń, Poland*
[2]*Kepler Institute of Astronomy, University of Zielona Góra, Lubuska 2, PL-65-265 Zielona Góra, Poland*
[3]*Institute of Astronomy, Bulgarian Academy of Sciences, 72 Tsarigradsko Chausse Blvd, BG-1784 Sofia, Bulgaria*
[4]*Max Planck Institute for Extraterrestrial Physics, Giessenbachstrasse, D-85748 Garching, Germany*
[5]*National Astronomical Research Institute of Thailand, 191 Siriphanich Bldg, Huay Kaew Rd, Suthep, Muang, Chiang Mai 50200, Thailand*
[6]*Instituto de Astrofísica de Canarias, C/ vía Láctea, s/n, E-38205 La Laguna, Tenerife, Spain*
[7]*Departamento de Astrofísica, Universidad de La Laguna, Av. Astrofísico Francisco Sánchez, s/n, E-38206 La Laguna, Tenerife, Spain*
[8]*Department of Physics, Faculty of Science, Atatürk University, Erzurum 25240, Turkey*

Accepted 2014 December 18. Received 2014 December 14; in original form 2014 August 19

ABSTRACT

We study the mid-egress eclipse timing data gathered for the cataclysmic binary HU Aquarii during the years 1993–2014. The (O−C) residuals were previously attributed to a single ∼7 Jupiter mass companion in ∼5 au orbit or to a stable two-planet system with an unconstrained outermost orbit. We present 22 new observations gathered between 2011 June and 2014 July with four instruments around the world. They reveal a systematic deviation of ∼60–120 s from the older ephemeris. We re-analyse the whole set of the timing data available. Our results provide an erratum to the previous HU Aqr planetary models, indicating that the hypothesis for a third and fourth body in this system is uncertain. The dynamical stability criterion and a particular geometry of orbits rule out coplanar two-planet configurations. A putative HU Aqr planetary system may be more complex, e.g. highly non-coplanar. Indeed, we found examples of three-planet configurations with the middle planet in a retrograde orbit, which are stable for at least 1 Gyr, and consistent with the observations. The (O−C) may be also driven by oscillations of the gravitational quadrupole moment of the secondary, as predicted by the Lanza et al. modification of the Applegate mechanism. Further systematic, long-term monitoring of HU Aqr is required to interpret the (O−C) residuals.

Key words: techniques: photometric – stars: individual: HU Aqr – novae, cataclysmic variables – planetary systems.

1 INTRODUCTION

The HU Aquarii binary system (HU Aqr hereafter) is one of the brightest polars discovered so far (Schwope, Thomas & Beuermann 1993; Warner 1995). This binary belongs to the class of magnetic cataclysmic variables (CVs). It consists of a strongly magnetized white dwarf (WD, primary component) and a main-sequence red dwarf (RD, M4V spectral type, secondary component). The RD fills its Roche lobe (Warner 1995). The spin periods of both components are synchronized with the short orbital period of ∼125 min by tidal forces and extremely strong magnetic fields. Since the discovery (Schwope et al. 1993), eclipses of HU Aqr have been monitored frequently by several groups and many different facilities. Because the mid-egress phase of the eclipses is very short, spanning a few seconds only, it is widely adopted in the literature as a standard eclipse time-marker. Already a decade ago, Schwope et al. (2001) reported deviations of the eclipse timing from the linear ephemeris (O−C).

A few physical phenomena intrinsic to the binary system, such as magnetic braking, mass transfer (Vogel et al. 2008; Schwarz et al. 2009), Applegate cycles (Applegate 1992), orbital precession of the binary (Parsons et al. 2014), the rigid body precession of the WD (Tovmassian, Zharikov & Neustroev 2007) and a migration of the accretion spot on the WD surface, are commonly ruled out to be the source of the (O−C) for HU Aqr (Vogel et al. 2008; Schwarz et al. 2009; Qian et al. 2011), see also the most recent analysis by Bours et al. (2014) and references therein. Instead, the (O−C) variations have been interpreted as the light travel time effect (LTT hereafter, or the Rømer effect) due to the presence of one or more massive, Jovian companions (Schwarz et al. 2009; Qian et al. 2011; Goździewski et al. 2012; Hinse et al. 2012b). A common problem

★ E-mail: k.gozdziewski@umk.pl

© 2015 The Authors
Published by Oxford University Press on behalf of the Royal Astronomical Society

Downloaded from http://mnras.oxfordjournals.org/ by guest on February 11, 2015

of multiple-planet models is their short-time dynamic instability spanning just 10^3–10^4 yr time-scales (Horner et al. 2011; Hinse et al. 2012b; Wittenmyer et al. 2012). This indicates that the common understanding of mechanisms driving the (O−C) in HU Aqr may be in fact incomplete. Indeed, Lanza et al. (1998), Lanza & Rodonò (1999, 2002, 2004) and Lanza (2005, 2006) derived a mechanism of the orbital period modulations in close binaries due to magnetic activity cycles in one component, extending the idea of Applegate (1992). This theory is build upon a hypothesis that the action of the hydromagnetic dynamo and the Lorentz force in the convective zone of the active star may cyclically change its quadrupole moment. This is sufficient for inducing the orbital period variability with only a fraction of the energy required by the simplified Applegate approach (Lanza et al. 1998; Lanza 2006), see also a note in Brinkworth et al. (2006).

In our previous paper (Goździewski et al. 2012), we demonstrated that planetary models of the (O−C) may be affected by a non-proper, kinematic formulation of the (O−C). Kinematic (Keplerian) models are unsuitable for strongly interacting, massive planets, presumably close to low-order mean motion resonances (MMRs). This is known at least since the remarkable paper by Laughlin & Chambers (2001) devoted to the radial velocity (RV) discoveries of extrasolar planets. The LTT and RV models have in fact a very similar mathematical formulation and concern similar mass ranges and orbital scales of planetary systems. Following this idea, in Goździewski et al. (2012), we introduced the self-consistent *N*-body model of the LTT effect. This Newtonian formulation revealed a continuum of *stable, two-planet configurations* of the HU Aqr system with an unconstrained outermost orbit.

We found that the parabolic ephemeris permitting such stable solutions must involve an excessively large secular decrease of the binary period. Only for stable two-planet configurations involved in low-order MMRs, like the 3:2 MMR, spanning narrow islands in the orbital elements space, we found the orbital period decrease to be reasonably small, though still two to three times larger than it is usually explained by magnetic braking, mass transfer or Applegate cycles, as argued by Vogel et al. (2008), Schwarz et al. (2009), Qian et al. (2011) and Bours et al. (2014); see however the note above and discussion in this paper. We suggested a possible solution of this paradox by selecting a homogeneous subset of light curves in the optical domain. We proposed that non-unique two-planet models in the literature might appear due to mixing timing data in different spectral domains (infrared, ultraviolet, X-rays). That proposition was reinforced by observations derived from the fast photometer OPTIMA. The OPTIMA photometry in the optical domain, spanning more than 10 years between 1999 and 2012, exhibits formal sub-second accuracy and the collected data revealed an apparently perfect, single period (O−C) variation of ∼40 s full amplitude. Combined with other optical measurements, it might be attributed to a single, massive Jovian planet of $\sim 7\, m_{\rm Jup}$ in an ∼5 au orbit, simultaneously minimizing the number of free parameters in the (O−C) model. However, shortly towards the end of the observing season 2012, we noticed significant deviations from the parabolic ephemeris in Goździewski et al. (2012). After observations during 2013 September it was already clear that the (O−C) exceed the LTT semi-amplitude of all the previous planetary models by more than a factor of 2, also ruling out the one-planet solution proposed in Goździewski et al. (2012). The credit of detecting the large (O−C) belongs chronologically to Schwope & Thinius (2014), who found it independently. Unfortunately, our one-planet (single-period) solution overemphasizes the subset of the optical data, and the timing variability due to spectral windows and different geometry of the eclipses appears as non-significant.

Table 1. HU Aqr observations with OPTIMA photopolarimeter in 2011 and 2012 with the 1.3-m telescope at the SKO (Crete, Greece) in white light. Dates are given for the time of the mid-egress times.

Cycle	Date	Airmass	Moon Phase (per cent)
76348	2011-06-18	1.5–1.7	86
76394	2011-06-22	1.5–1.6	52
76395	2011-06-23	1.5–1.6	52
76406	2011-06-24	1.8–1.5	45
76464	2011-06-29	1.6–1.5	6
76532	2011-07-04	1.8–1.5	47
76555	2011-07-06	1.9–1.5	35
76556	2011-07-07	1.9–1.5	35
76567	2011-07-07	1.55–1.6	47
76648	2011-07-15	1.7–1.55	100
81001	2012-07-26	1.55–1.48	57
81013	2012-07-28	1.5–2.2	68
81162	2012-08-09	1.52–1.47	48
81186	2012-08-12	1.74–1.84	21
81231	2012-08-15	1.52–1.55	3

Therefore, we found it necessary to conduct a new analysis of the up-to-date set of all observations and to revise all LTT models derived so far (Schwarz et al. 2009; Qian et al. 2011; Goździewski et al. 2012; Hinse et al. 2012b). Since the *N*-body two-planet models in Goździewski et al. (2012) were constructed on the basis of *all* available data, we continue the previous work, providing also an erratum to this paper. We stress here, that we test the LTT hypothesis in detail, as one of possible causes of the (O−C) variability, recalling that the Lanza (2006) theory might also explain the (O−C), without invoking the Rœmer effect at all.

During corrections of this manuscript in accord with the reviewer's report, we found that Bours et al. (2014) reported new 22 precision measurements of the HU Aqr spanning essentially the same time period, as data gathered in our paper. Our work extends the results of Bours et al. (2014), since we focus on the detailed analysis of the planetary models. We prove that the source of strong dynamical instability in the HU Aqr planetary systems are similar semimajor axes, placing putative companions of the binary in a region of the 1:1 MMR and 3:2 MMR, combined with large and unconstrained masses.

In this paper, we gathered the new measurements in the originally submitted manuscript and the new observations published by Bours et al. (2014). We verified that the results obtained without and with their measurements, respectively, differ only up to quantitative sense (i.e. the best-fitting parameters are slightly altered). With the aim of publishing the most up-to-date results possible, we re-analysed available timing data of the HU Aqr eclipses, which are collected in the appendix.

This paper is structured as follows. Section 2 presents 22 new observations of HU Aqr carried out between 2011 and 2014. This set comprises of light curves gathered with the OPTIMA photopolarimeter hosted by the Skinakas Observatory (SKO, Crete, Greece), as well as the most recent data taken with 2D detectors operated in three different observatories, see Tables 1 and 2 for details. Section 3 is devoted to the Keplerian and Newtonian (O−C) models. We compare the results from the kinematic and self-consistent *N*-body models of the LTT effect. Even more arguments are given against the kinematic model of separate LTT orbits (Irwin 1952), which is common in the recent literature (e.g. Qian et al. 2011; Beuermann et al. 2012; Hinse et al. 2012b; Almeida, Jablonski & Rodrigues 2013; Hinse, Horner & Wittenmyer 2014; Lee et al. 2014). We

Downloaded from http://mnras.oxfordjournals.org/ by guest on February 11, 2015

Table 2. Parameters and conditions of HU Aqr observations with CCD detectors. The observatory abbreviations are provided in the text, while the filters abbreviations stand for 'Cl' – clear, 'L' – clear and 'g'' – standard SDSS filter, respectively. 'Expos.' – stands for the exposure time. Readout time and airmass are also given.

Cycle	Date	Obs./ Filter	Expos. (s)	Readout (s)	Airmass
85746	2013-09-11	NAO/Cl	10	∼ 4	1.55–1.70
86032	2013-10-06	NAO/Cl	3	∼ 0.5	1.54–1.47
86412	2013-11-08	NAO/Cl	3	∼ 0.5	1.47–1.76
86976	2013-12-27	COG/L	15	∼ 5	2.10–2.66
88383	2014-04-28	TNO/g'	4.35	∼ 0	1.80–1.60
89339	2014-07-20	NAO/Cl	3	∼ 2.5	2.30–2.00
89340	2014-07-20	NAO/Cl	3	∼ 2.5	1.50–1.45

Table 3. New HU Aqr BJD mid-egress times on the basis of light curves collected with the OPTIMA photometer operated at the Skinakas Observatory (OPT–SKO), with 2-m telescope at the National Astronomical Observatory (PIVA–NAO), with PW24 at the Campus Observatory Garching (PW24–COG), as well as with the ULTRASPEC camera at 2.4-m Thai National Telescope (ULTRA-TNT).

Cycle L	BJD	Error (d − s)	Instrument
76348	2455731.4841422	0.000 0054−0.47	OPT–SKO
76394	2455735.4778822	0.000 0025−0.22	OPT–SKO
76395	2455735.5646948	0.000 0023−0.20	OPT–SKO
76406	2455736.5197228	0.000 0019−0.16	OPT–SKO
76464	2455741.5552777	0.000 0093−0.80	OPT–SKO
76532	2455747.4590878	0.000 0029−0.25	OPT–SKO
76555	2455749.4559585	0.000 0017−0.15	OPT–SKO
76556	2455749.5427747	0.000 0016−0.14	OPT–SKO
76567	2455750.4978035	0.000 0019−0.16	OPT–SKO
76648	2455757.5302482	0.000 0071−0.61	OPT–SKO
81001	2456135.4591635	0.000 0071−0.61	OPT–SKO
81013	2456136.5010300	0.000 0058−0.50	OPT–SKO
81162	2456149.4372694	0.000 0059−0.51	OPT–SKO
81186	2456151.5209490	0.000 0020−0.17	OPT–SKO
81231	2456155.4278501	0.000 0034−0.29	OPT–SKO
85746	2456547.4214776	0.000 0073−0.63	PIVA-NAO
86032	2456572.2520793	0.000 0034−0.29	PIVA-NAO
86412	2456605.2437774	0.000 0027−0.24	PIVA-NAO
86976	2456654.2104280	0.000 0361−3.12	PW24-COG
88383	2456776.3665044	0.000 0017−0.14	ULTRA-TNT
89339	2456859.3666325	0.000 0064−0.56	PIVA-NAO
89340	2456859.4534517	0.000 0103−0.89	PIVA-NAO

discuss the dynamical stability of Newtonian solutions in Section 3.7 and we conclude that at present, coplanar two-planet and three-planet models with direct orbits are unlikely to explain the recent (O−C) data of HU Aqr. We show that stable three-planet systems with highly inclined orbits are possible. We discuss the results in Section 4, estimating the (O−C) amplitude due to the modified Applegate mechanism, and we propose independent astrometric and imaging observations to verify the LTT hypothesis. The appendix contains a compilation of the data set used in this paper.

2 NEW PHOTOMETRY OF HU AQR

2.1 Observations with OPTIMA in 2011 and 2012

There are 22 unpublished and new mid-egress times listed in Table 3. Among them, 15 data points were obtained with the high time resolution photo-polarimeter OPTIMA[1] (Straubmeier, Kanbach & Schrey 2001; Kanbach et al. 2008; Stefanescu 2011). OPTIMA was initially designed for optical pulsar studies; however, it is not limited to this subject only. Examples of results obtained with OPTIMA include e.g. pulsars (Słowikowska et al. 2009), the first optical magnetar (Stefanescu et al. 2008), intermediate polars (Nasiroglu et al. 2012), polars (Słowikowska et al. 2013) and a black hole candidate with optical variability (Kanbach et al. 2001).

Similar to previous years, we have conducted several observations of HU Aqr during our OPTIMA observing campaigns at the SKO in 2011 and 2012 (Goździewski et al. 2012; Słowikowska et al. 2013). Obtained light curves are shown in Fig. 1. Using fibre-fed single photon counters, OPTIMA is capable of recording single optical photons with an internal accuracy of 5 ns. The absolute timing accuracy of the GPS signal is of the order of ∼20–40 ns. For the purpose of this paper, we bin the OPTIMA counts for 1 s time resolution. This is sufficient to determine the mid-egress moment very accurately, with formal sub-second time precision. (We carefully checked that binning with interval of 1–3 s does not change the results; hence, we choose the 1 s bins to obtain denser sampling of the light curves). Technical information about the observations is gathered in Table 1.

2.2 CCD-based observations in 2013 and 2014

In 2013 and 2014, we performed observations at the National Astronomical Observatory in Rozhen (NAO, Bulgaria) and at the Campus Observatory Garching (COG, Germany). We also observed HU Aqr with the recently inaugurated 2.4-m Thai National Telescope (TNT) at the Thai National Observatory (TNO, Thailand), equipped with the ULTRASPEC instrument (Dhillon et al. 2014). Technical information about the observations is gathered in Table 2.

Around the middle of the year 2014, we also derived a few light curves with the PTST 24 inch telescope at the Observatorio Astronómico de Mallorca (OAM, Spain) as well as the FastCam instrument (Oscoz et al. 2008) at the Teide Observatory (TO, Spain) where we used the 1.55-m Telescopio Carlos Sánchez (TCS, Spain). The most recent observations were performed on 2014 July 23–26 at the TÜBİTAK National Observatory (TUG, Turkey) with a 1-m robotic telescope. Unfortunately, these data have relatively low photometric quality and are skipped in this paper.

The main telescope of the NAO Rozhen is a 2-m Ritchey–Chretien–Coudé reflector equipped with the Princeton Instruments VersArray (PIVA): 1300 CCD camera that has a resolution of 580 × 550 pixels (pixel physical size of 20 μm, image scale 0.258 arcsec pixel^{-1} and the field of view FoV 2.5 arcmin × 2.36 arcmin). The camera is cooled down to −110°C. Light curves obtained with the 2-m NAO telescope are shown in Fig. 2.

At the TNT 2.4-m telescope we used ULTRASPEC (Dhillon et al. 2014), an LN_2-cooled frame-transfer EMCCD with a 1024 × 1024 active detector area which is designed for fast, low-noise operation. Thanks to the use of subarray windows high frame rates can be achieved, up to few 10^2 Hz (Richichi et al. 2014). Each frame is time-stamped at mid-exposure with a dedicated GPS system. The internal timing accuracy of the system has been tested to better than 1 ms. The observation was carried out in a standard SDSS g' filter. The resulting light curve is shown in Fig. 2.

[1] http://www.mpe.mpg.de/OPTIMA

Downloaded from http://mnras.oxfordjournals.org/ by guest on February 11, 2015

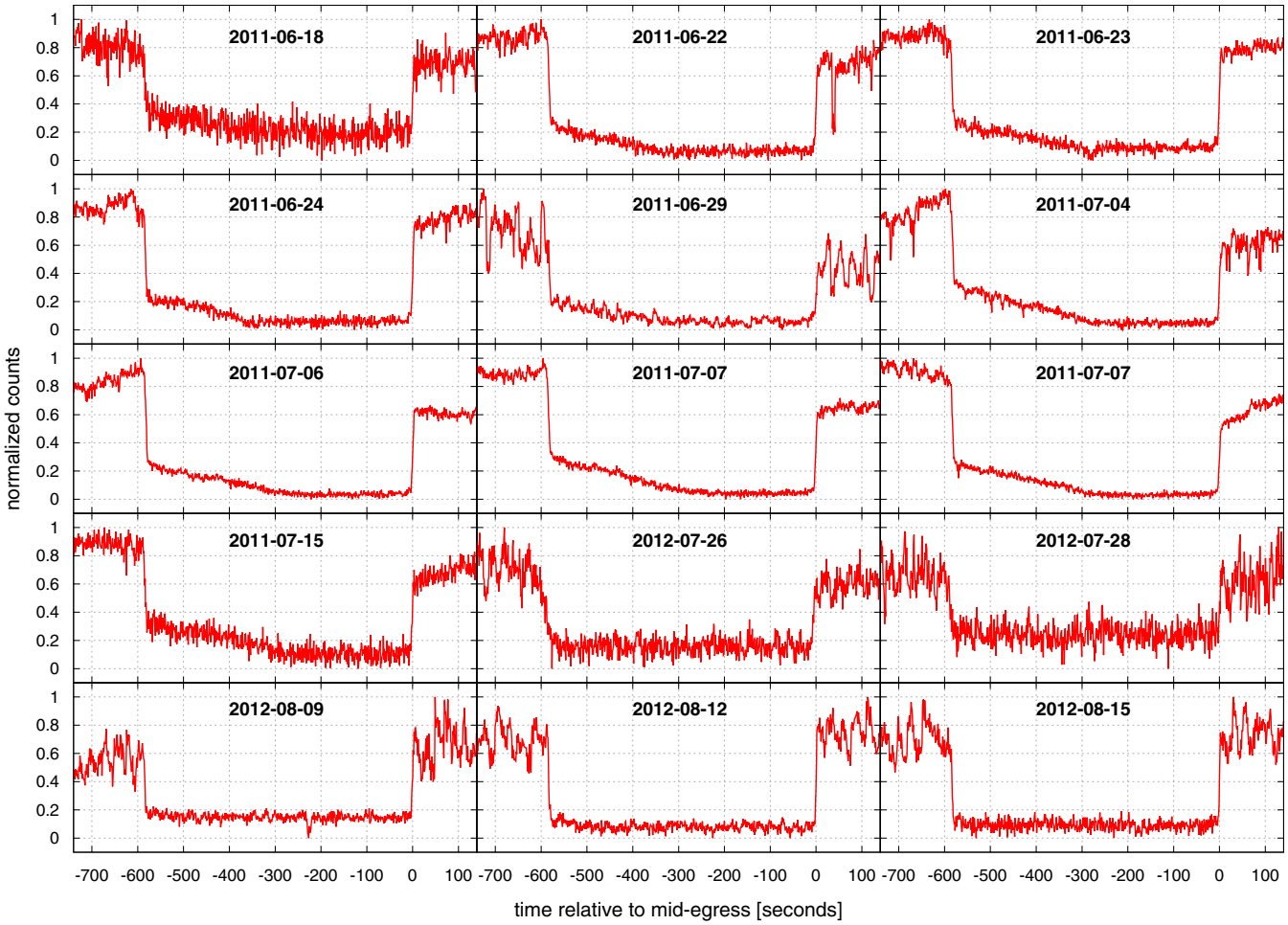

Figure 1. The normalized light curves of HU Aqr obtained with OPTIMA in 2011 and 2012 (OPT-SKO). Time at the *x*-axis is relative the mid-egress moment, in accord with Table 3.

2.3 Data analysis and timing accuracy

The CCD data were reduced with the IRAF package; for NAO observations the bias and flat-field corrections were applied, while in the case of COG data only dark frames were subtracted. The TNO observations were reduced with the ULTRACAM data reduction pipeline v9.12[2], a dedicated software for calibration and aperture photometry analysis of the data gathered by ULTRACAM and ULTRASPEC instruments. In all cases, special care of the timing accuracy was taken. In the case of OPTIMA timing is achieved by using a GPS receiver. In the case of NAO, the system time is synchronized automatically every 10 min with a GPS receiver and information for corrections is saved in a log file. Additionally, it was later controlled through NTP server http://time.nist.gov and the difference was always smaller than 0.2 s. Time is updated every 15 min on COG at ntp2.mpe.mpg.de via SNTP (MPE). Data were time stamped as JD UTC, and for the CCD data the mid-exposure times were taken.

To derive the mid-egress moment, the sigmoid function representing the photometric flux:

$$I(t) = a_1 + \frac{a_2 - a_1}{1.0 - \exp([t_0 - t]/\Delta t)}, \quad (1)$$

(where a_1, a_2, Δt are parameters describing the sigmoid shape), was fitted to selected light curves around the mid-egress moment t_0, within some range of time t. This procedure is described in section 4.2 of Goździewski et al. (2012). Then the derived UTC mid-egress moments were converted to the BJD (Barycentric Dynamical Time), using the ICRS sky coordinates of HU Aqr and the geodetic coordinates of each given observatory, with the help of a numerical procedure developed by Eastman, Siverd & Gaudi (2010). For all mid-egress data, we adopted the formal 1σ error of the parameter t_0. The mid-egress times obtained with all mentioned telescopes and instruments are listed in Table 3.

3 LTT MODELS OF THE (O−C)

To revise the LTT models of Goździewski et al. (2012), we use the collected mid-egress moments published in Schwope et al. (2001), Schwarz et al. (2009), Goździewski et al. (2012), updated by our new observations displayed in Table 3 and by the recent 22 data points published by Bours et al. (2014). Summarizing the new 44 data points extend the set of all previous literature data used for constraining *N*-body models in Goździewski et al. (2012). A complete list of 215 mid-egress moments is compiled in the appendix (Table A1). The zero cycle ($L = 0$) epoch for the third body models is $T_0 =$ JD 245 3504.888 294 00, roughly in the middle of the observation window, and of the most accurate OPTIMA measurements.

[2] http://deneb.astro.warwick.ac.uk/phsaap/software/ultracam/html/

Downloaded from http://mnras.oxfordjournals.org/ by guest on February 11, 2015

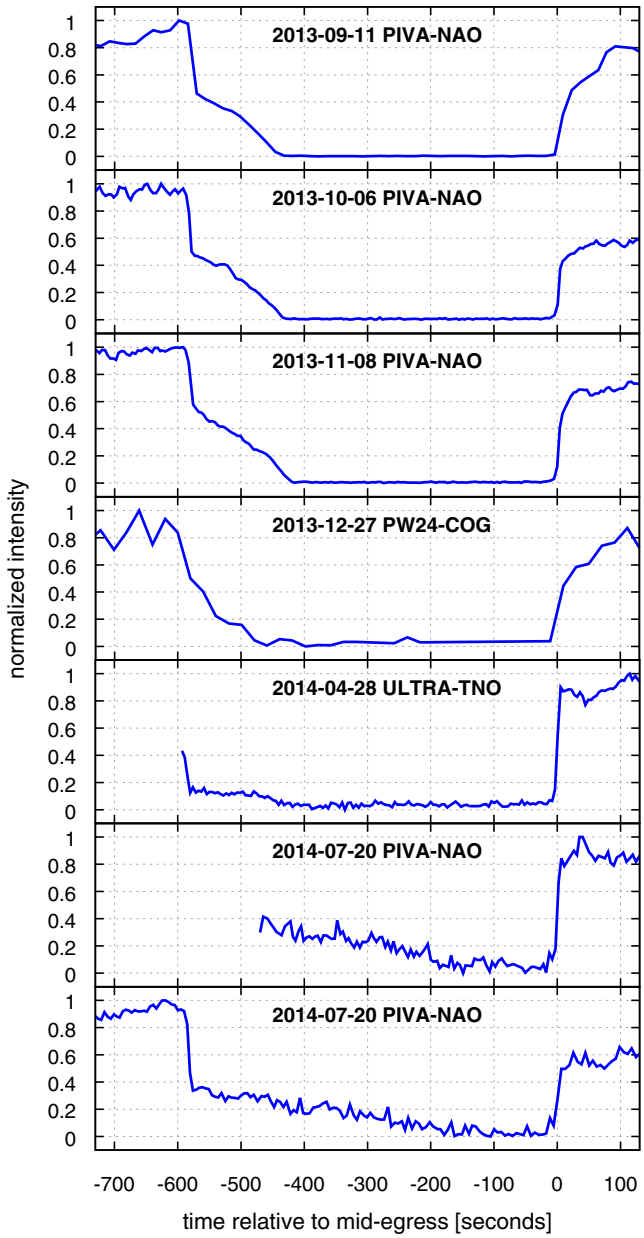

Figure 2. The light curves of HU Aqr obtained with various CCD instruments: with the 2-m Rozhen telescope (PIVA-NAO) in 2013 during the nights of September 11, October 6 and November 8 and two eclipses obtained in 2014, July 20; from PW24-COG (2013 December 27) and from ULTRASPEC/TNO (2014 April 28). Time at the *x*-axis is relative the mid-egress moment, in accord with Table 3.

Note that Table A1 displays eclipse cycles counted from epoch JD 244 9102.920 0026, i.e. the epoch of first observation of HU Aqr in Schwope et al. (1993). Though the mid-egress measurements in Qian et al. (2011) are included in Table A1, they are not used here. These data systematically outlay by a few seconds from more accurate OPTIMA and MONET/N timings, spanning the same observational window (Goździewski et al. 2012). Note that Bours et al. (2014) also did not include the Qian et al. (2011) observations for the same reason.

With these data, we construct (O−C) diagrams (Fig. 3) for the linear and parabolic ephemeris, respectively,

$$T_{\rm ephem}(L) = t_0 + L P_{\rm bin} + \beta L^2, \qquad (2)$$

where $T_{\rm ephem}(L)$ is the time of predicted mid-egress at eclipse cycle L, t_0 is the epoch and β is the derivative of the orbital period $P_{\rm bin}$, in accord with Hilditch (2001).

Significant (O−C) mid-egress deviations from the linear ephemeris (blue filled circles in Fig. 3, the left-hand panel) and from the parabolic ephemeris (red filled circles in the right-hand panel) have become apparent shortly after the end of observing season 2012 (see at the left border of shadowed rectangles). We continued to monitor the target in 2013 September (NAO, Rozhen). Around this epoch, the (O−C) for the parabolic ephemeris in Goździewski et al. (2012) are already ∼60 s. Such a large magnitude was very unexpected, and we tried to verify and confirm the NAO timing data with other instruments. It was possible only in 2013 December through observations with the PW24-COG instrument (see Table 2). Shortly thereafter, Schwope & Thinius (2014) published six observations performed with a small 14 inch Celestron telescope, between October 22 and 30, and new ephemerides of the HU Aqr eclipses. (We do not use their observations in this paper due to low quality lightcurves.) Continued monitoring of the HU Aqr during the new observing season 2014 revealed progressing decay of (O−C). Recent (O−C) reach 120 s for the linear ephemeris, and more than 60 s for the parabolic ephemeris (Fig. 3). The parabolic term about of -5×10^{-13} day L^{-2} is larger than its previous estimates (e.g. Schwarz et al. 2009; Qian et al. 2011; Goździewski et al. 2012).

3.1 Keplerian model of the LTT and optimization algorithms

In Goździewski et al. (2012), we revised a common kinematic (Keplerian) formulation of the LTT effect (Irwin 1952) for multiple companions of the binary. This is accomplished by expressing eclipse ephemerides w.r.t. Jacobi coordinates with the origin at the centre of mass (CM) of the binary. Because the binary period is shorter than the orbital periods by a factor of $\sim 10^5$, the binary is well approximated by a point in the CM with the total mass of both stars; the mass of the HU Aqr binary is 0.98 $M_\odot$ (Schwope et al. 2011). Osculating orbital elements and masses derived in this way best match the true, *N*-body initial condition of the system with mutually interacting planets.

This ephemeris model accounting for the presence of planetary companions has the more general form of equation (2):

$$T_{\rm ephem}(L) = t_0 + L P_{\rm bin} + \beta L^2 + \sum_p \zeta_p(t(L)), \qquad (3)$$

where the $\zeta_p(t)$ terms are for the (O−C) deviations induced by gravitational perturbation of the CM by the third bodies ($p = 1, 2, \ldots$ or, in accord with the common convention $p = \mathrm{b}, \mathrm{c}, \ldots$):

$$\zeta_p(t) = K_p \left[\sin\omega_p(\cos E_p(t) - e_p) + \cos\omega_p \sqrt{1 - e_p^2} \sin E_p(t) \right],$$

and K_p, e_p, ω_p are the semi-amplitude of the LTT signal, eccentricity and argument of the pericentre, respectively, for body p. Its orbital period P_p and the pericentre passage T_p are introduced indirectly through the eccentric anomaly $E_p(t)$. Details are given in Goździewski et al. (2012), see also further development of this idea and discussion in Marsh et al. (2014).

The initial (O−C) diagrams in Fig. 3 are suggestive for a significant parabolic term, which is also often quoted in the literature. Therefore, we optimized the general form of equation (3) including a parameter β that accounts for a secular change of the binary period $P_{\rm bin}$ (i.e. the quadratic ephemeris). After extensive analysis, we found that an alternative two-planet model with the linear ephemeris is heavily unconstrained with respect to a few parameters. Its formal

Downloaded from http://mnras.oxfordjournals.org/ by guest on February 11, 2015

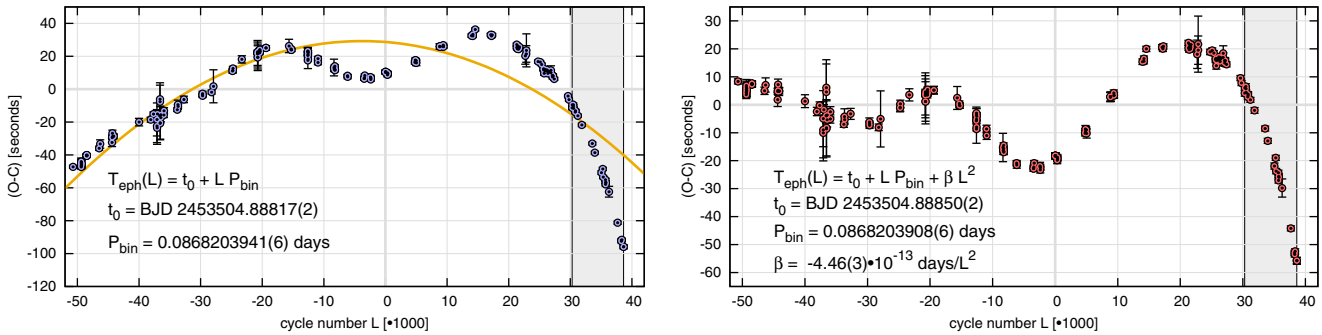

Figure 3. The (O−C) diagrams for mid-egress moments of HU Aqr collected in this paper (see the appendix, Table A1), with the 'jitter' error correction of $\sigma_{\rm f} = 0.9$ s, see the text for details. Red and blue filled circles are for the linear (the left-hand panel) and for parabolic (the right-hand panel) ephemeris, respectively. The yellow curve in the left-hand panel illustrates the parabolic term in equation (2). Labels are for the fitted parameters to equation (2) with uncertainties at the last significant digit, which is marked with a digit in parenthesis. The shaded region is for the new data that show a large deviation from the previous predictions in the literature.

best-fitting solution has similar orbital periods ∼22 yr, and permits LTT semi-amplitudes $K_{1,2}$ as large as 60 min. This implies the non-physical companion masses of $\sim 1\,{\rm M}_{\odot}$ (this will be shown at the end of this section). Moreover, the linear ephemeris model provides statistically worse solutions in terms of an rms, as compared to the two-planet quadratic ephemeris, i.e. the fit model with only one free parameter more. The quadratic term, usually interpreted as the binary period derivative (Hilditch 2001), might be also caused by a distant and massive companion with a very long orbital period. Hence, we focus mainly on the parabolic ephemeris variant of the two-companion hypothesis.

To optimize the ephemeris models in equation (3) in terms of the reduced χ^2_ν function, we apply a combination of the Genetic Algorithms (GA, Charbonneau 1995) and the local and fast Levenberg–Marquardt scheme, as described in Goździewski et al. (2012). This hybrid algorithm (HA from hereafter) provides an efficient and robust exploration of multidimensional parameter space. Each run of the HA starts from the GA step, which searches for reasonable solutions over wide ranges of model parameters. In particular, the hypercube of parameters explored by the GA has $K_{\rm b,\,c} \in [1, 1800]$ s, $P_{\rm b,\,c} \in [2000, 36\,000]$ d, $e_{\rm b,\,c} \in [0, 0.99]$, and all angles permitted in their full ranges. All GA-derived sets of solutions are then refined with the Levenberg–Marquardt method. This procedure repeated many times makes it possible to gather large statistics of solutions which are consistent with the observations. (HA may be also used to optimize the *N*-body models.)

3.2 Correction of the timing uncertainties

At the preliminary stage, we found that in spite of a wider observational window than in Goździewski et al. (2012), the HA converged to non-unique solutions with marginally different χ^2_ν. The best-fitting solutions exhibit $\chi^2_\nu \sim 9$ on the raw data in Table A1. Such a large value may indicate an incorrect fit model. However, recalling the quasi-periodic character of the (O−C) shown in Fig. 3 and astrophysical arguments, we assumed that the LTT model may be valid. Therefore, the second possibility are underestimated uncertainties of the measurements (Bevington & Robinson 2003). This makes it difficult to derive proper uncertainties of the fit parameters. Hence, assuming that the mid-egress errors are normally distributed, we examined the uncertainty correction, similar to the so-called stellar jitter, which is a well-known factor that must be accounted for in the RV technique (e.g. Butler et al. 2003; Wright 2005). In simple settings, a one-parameter jitter uncertainty describes intrinsic RV variability that is caused by the stellar chromosphere. Here, we consider a similar correction to the mid-egress timing error, which accounts, for instance, for the unmodelled geometry of eclipses, or observational circumstances and instrumental errors, e.g. additional elements of emission or absorption of light in the binary system. We add such a priori unspecified term $\sigma_{\rm f}$ in quadrature to uncertainties of individual observations σ_i, through $\sigma_i^2 \rightarrow \sigma_i^2 + \sigma_{\rm f}^2$, where $i = 1, \ldots, N_{\rm obs}$, and $N_{\rm obs}$ is the total number of measurements. The $\sigma_{\rm f}$ term is then the free parameter of the fit model.

The introduction of the $\sigma_{\rm f}$ factor is supported by arguments of Schwope & Thinius (2014). They argue that formal uncertainties of the mid-egress moments below ∼1 s are much smaller than the finite physical size of the accretion spot. The X-ray emitting region is ∼450 km across wide (Schwope et al. 2001), and is wider in the optical domain since the egress phase lasts for ∼7–8 s. Moreover, the accretion area migrates over the WD surface, hence the geometry of eclipses is changing, and introducing a short-term component of the (O−C), which is estimated for 1–2 s (Schwarz et al. 2009). Small timing errors are possible for densely sampled light curves, and are reported, for instance, by Schwope et al. (2001) for *ROSAT* (quoted errors for cycles 2212–2225 are ∼0.13–0.24 s), by Goździewski et al. (2012) for OPTIMA data (quoted errors are on the level of ∼0.1–0.8 s), by Schwarz et al. (2009) for UTRACAM-VLT (errors ∼0.5 s), and, very recently by Bours et al. (2014) for the ULTRASPEC-TNT instrument (the quoted errors are as small as 0.02–0.06 s).

To determine $\sigma_{\rm f}$ for selected solutions found with the HA, we optimized the maximum likelihood function $\mathcal{L}$:

$$\log \mathcal{L} = -\frac{1}{2}\sum_i \frac{({\rm O{-}C})_i^2}{(\sigma_i^2 + \sigma_{\rm f}^2)} - \sum_i \log\sqrt{\sigma_i^2 + \sigma_{\rm f}^2} - N \log\sqrt{2\pi}, \tag{4}$$

where $({\rm O{-}C})_i$ is the (O−C) deviation of the mid-egress at given eclipse cycle L_i (equation 3). This form of $\mathcal{L}$ is similar to that one introduced by Baluev (2008) for the RV data.

Furthermore, to analyse the parameter correlations in detail, we performed the Markov Chain Monte Carlo (MCMC) analysis of selected best-fitting solutions. The posterior probability distribution of model parameters $\boldsymbol{\theta}$ given the data set $\mathcal{D}$ is defined through

$$p(\boldsymbol{\theta}|\mathcal{D}) \propto p(\boldsymbol{\theta})p(\mathcal{D}|\boldsymbol{\theta}),$$

where $p(\boldsymbol{\theta})$ is the prior, and the sampling data distribution $p(\mathcal{D}|\boldsymbol{\theta}) \equiv \log \mathcal{L}(\boldsymbol{\theta}, \mathcal{D})$. We defined the parameter priors as uniform or uniform

Downloaded from http://mnras.oxfordjournals.org/ by guest on February 11, 2015

improper through placing only natural, physical and geometric limits on the parameters, i.e. $K_p > 0$, $P_p > 0$, $e_p \in [0, 1)$, $\omega_p \in [0, 2\pi]$, $T_p > 0$, $P_{bin} > 0$, $\beta < 0$, and $\sigma_f > 0$, where p is the planet index, p = b, c, d, and so on. These computationally simple priors are justified here, since we analyse well localized solutions. Moreover, we verified that the modified Jeffreys prior for parameter $\theta \equiv \sigma_f$, as introduced by Gregory (2005),

$$p(\theta) = \frac{1}{(\theta + \theta_{min})} \frac{1}{\log[(\theta_{min} + \theta_{max})/\theta_{min}]},$$

(where θ_{min} and θ_{max} are scaling constants, fixed for σ_f as equal to 0.01 s and 10 s, respectively), does not change the results. Similar priors have been defined for the N-body models, with planetary masses $m_p > 0$, semimajor axes $a_p > 0$, eccentricities $e_p \in [0, 1)$, and all Keplerian angles $\in [0, 2\pi]$.

To perform the optimization of $\log \mathcal{L}$ and the MCMC analysis, we prepared PYTHON interfaces to model functions written originally in FORTRAN and we used publicly available, excellent EMCEE code of the affine-invariant ensemble sampler for MCMC proposed by Goodman & Weare (2010), kindly provided by Foreman-Mackey et al. (2013). See also the recent paper by Marsh et al. (2014) for a consistent application of the MCMC optimization and this code to the analysis of the (O−C) diagrams.

As shown below, all LTT models of HU Aqr studied in this paper suffer from strong parameter correlations and are not unique (the posteriors are multimodal). In such a case, an efficient application of the MCMC to explore the whole parameter space is very difficult (Foreman-Mackey et al. 2013; Marsh et al. 2014). In this sense, we found that the HA and MCMC are complementary. The MCMC method is a great tool to analyse properties of the best-fitting configuration found with the HA, and is very useful to derive realistic uncertainties of the parameters.

The results for the best-fitting Keplerian two-planet quadratic ephemeris model (Table 4) are illustrated in the form of 1D and 2D projections of the posterior probability distributions. The best-fitting models obtained in this way have slightly altered parameters, as compared to their values derived through standard minimization of χ^2_ν. We obtained $\sigma_f \sim 0.9$–1.5 s for different LTT variants (i.e. two-planet and three-planet configurations with the linear and parabolic ephemeris) and the most recent data set. After applying the correction term, we found that χ^2_ν is ∼1, and the rms remains unaltered, as expected. Furthermore, we ran the HA optimization code on all mid-egress data in Table A1, with uncertainties added in quadrature to a constant value of $\sigma_f = 0.9$ s. Yet individual best-fitting models were recomputed with σ_f as a free parameter. The σ_f correction is most significant for *ROSAT*, OPTIMA and ULTRASPEC measurements with formal sub-second accuracy. (Note, that mid-egress timing data in Table A1 do not include this term in the error column.)

It may be easily overlooked that the error correction has a significant influence on the parabolic ephemeris itself, see the right-hand panel in Fig. 3, which shows the (O−C) diagram computed for data errors corrected with $\sigma_f = 0.9$ s. Without this correction, $\beta \simeq -5.4 \times 10^{-13}$ d L^{-2}, and the residual (O−C) signal to be explained by the LTT model is clearly modified, when compared to the raw timing data.

3.3 Quadratic ephemeris, kinematic two-planet model

The resulting set of HA-derived solutions to the two-planet quadratic ephemeris is illustrated as projections of their parameters on to selected planes in Fig. 4. This set reveals a shallow minimum of $\chi^2_\nu \sim 1.0$ and an rms∼1.8 s. However, the set of formal 1σ solutions providing $\chi^2_\nu < 1.04$ forms a narrow 'valley' in particular planes. This indicates that the Keplerian model is unconstrained. The 1σ-solutions might be divided into two groups. The first group is characterized with $K_{b,c} \sim 30$–60 s and bounded orbital periods locating putative two-planet systems close to the 3: 2 MMR. The best-fitting model JQ of this type is illustrated in the right-hand panel of Fig. 5, see Table 4. The second group of models reveals an apparently well-bounded inner orbital period $P_b \sim 4800$ d, but the outermost orbital period P_c is unconstrained, and it may be as large as 36 000 d and longer. This is correlated to the LTT semi-amplitude K_c up to 600 s. The inferred mass of the outermost companion may be as large as 80 m_{Jup} and larger. Formal uncertainties of Fit JQ in Table 4 are determined with the help of the MCMC analysis of the optimization model including the σ_f correction as a free parameter, in accord with equation (4).

An inspection of Fig. 4 reveals strong correlations between the parameters. This is particularly well visible in the (P_c, e_c)- and (P_c, β)-planes. A similar correlation is also found by Marsh et al. (2014) for the two-planet parabolic ephemeris of NN Ser (let us note that the residuals to the linear ephemeris of NN Ser are qualitatively similar to the HU Aqr case, recently showing a phase of fast increase after initially quasi-periodic oscillations). We investigated its nature with an independent method, by performing the MCMC analysis of Fit JQ (Fig. 6). Besides the (P_c, e_c)- and (P_c, β)-correlations, there is also a strong correlation between the orbital periods and the time of pericentre passage for each orbit (not shown here). Moreover, even in the smallest range, the β term has a large magnitude of -1×10^{-12} d L^{-2}, making the kinematic model questionable due to the unknown origin of such a large period derivative.

Table 4. Keplerian parameters in accord with two-planet LTT fit model with parabolic ephemeris to all available data in Table A1. Synthetic curves of these solutions with mid-egress times are illustrated in Fig. 5. Numbers in parentheses are for the uncertainty at the last significant digit. Total mass of the binary is 0.98 $M_\odot$ (Schwope et al. 2011). T_0 = JD 245 3504.888 2940 is the adopted osculating epoch coinciding with the $L = 0$ epoch, close the middle of observational window.

Parameters	Fit JQ	Fit JL
K_b (s)	33.6 ± 1.9	2765.6 ± 331.5
P_b (d)	4707.4 ± 19.0	8029.4 ± 18.2
e_b	0.270 ± 0.022	0.317 ± 0.015
ω_b (deg)	44.640 ± 8.0	206.2 ± 4.1
T_b [T_0+]	3845.4 ± 357.35	2917.4 ± 5524.6
a_b (au)	5.48	–
$m_b \sin i$ (m_{Jup})	12.7	–
K_c (s)	87.7 ± 4.0	2860.7 ± 337.2
P_c (d)	7101.7 ± 25.6	8298.8 ± 19.8
e_c	0.159 ± 0.014	0.336 ± 0.014
ω_c (deg)	346.2 ± 5.2	25.03 ± 4.0
T_c [T_0+]	3784.5 ± 1576.0	3714.1 ± 5766.5
a_c (au)	7.14	–
$m_c \sin i$ (m_{Jup})	25.8	–
P_{bin} (d)	0.868 203 6931(4)	0.086 820 3618(6)
t_0 [BJD 2,453,504.0+]	0.888 99(1)	0.887 42(15)
β [$\times 10^{-12}$ day$\cdot L^{-2}$]	−1.30(4)	–
σ_f (s)	0.92(8)	1.48(9)
N_{obs} data	205	205
χ^2_ν	0.96	1.04
rms (s)	1.72	2.02

Downloaded from http://mnras.oxfordjournals.org/ by guest on February 11, 2015

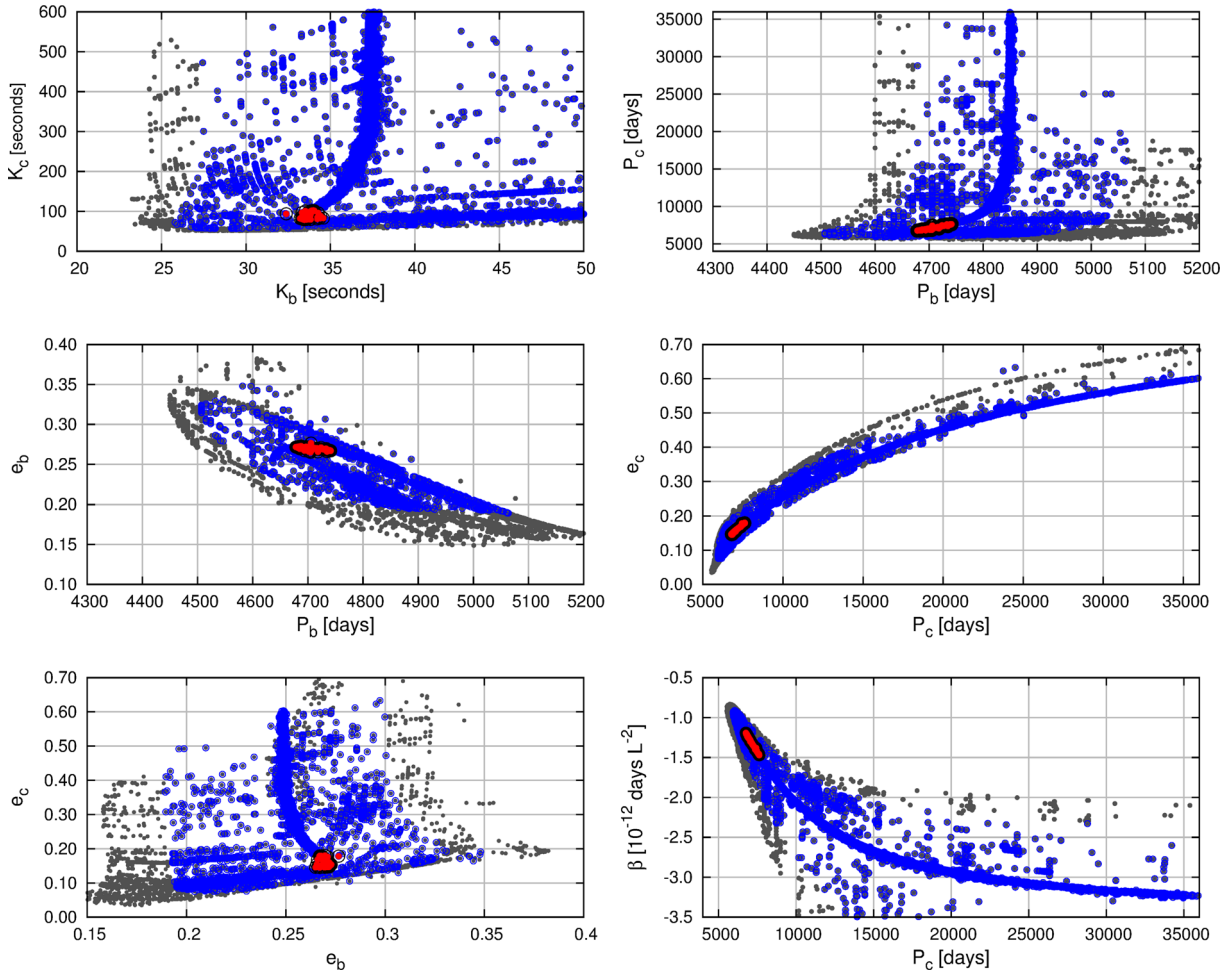

Figure 4. Best-fitting two-planet Jacobian solutions to the quadratic ephemeris projected on to selected parameter planes. Red circles are for models with $\chi^2_\nu < 0.99$ (marginally better than $\chi^2_\nu = 0.986$ of the best-fitting model JQ see Table 4), blue open circles and grey filled circles are for $\chi^2_\nu < 1.04$ and $\chi^2_\nu < 1.08$, respectively (roughly 1σ and 3σ-confidence intervals of the best-fitting solution).

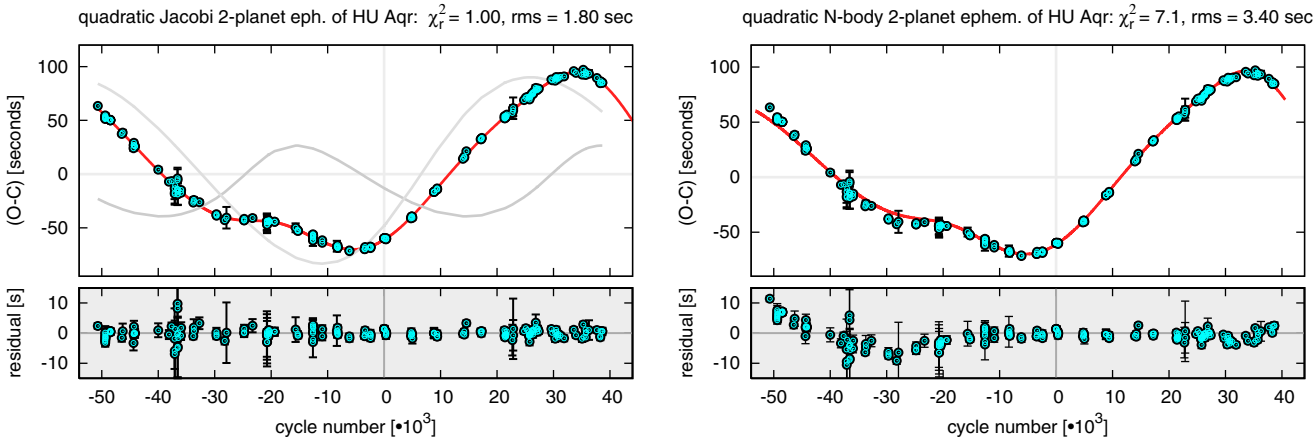

Figure 5. Best-fitting two-planet Jacobian solution (Fit JQ), left-hand panel. This model includes the quadratic term, see Table 4 for parameters of this fit. Shaded curves are for the individual LTT components, respectively. Right-hand panel: *N*-body synthetic curve for the osculating initial condition derived through the formal transformation of the Jacobian elements JQ to the *N*-body Cartesian osculating frame, centred at the CM of the binary.

3.4 Linear ephemeris, kinematic two-planet model

For reference, we also investigated the two-planet linear ephemeris model, which is a very 'attractive' variant of the LTT hypothesis. A stable system consistent with the linear ephemeris and observations would essentially solve the problem of large orbital period derivative β. Unfortunately, the linear model is even less constrained than the quadratic ephemeris case. The best-fitting solution found after an extensive HA search provides $\chi^2_\nu \sim 1.04$ and an rms $\sim$2.1 s. It

Downloaded from http://mnras.oxfordjournals.org/ by guest on February 11, 2015

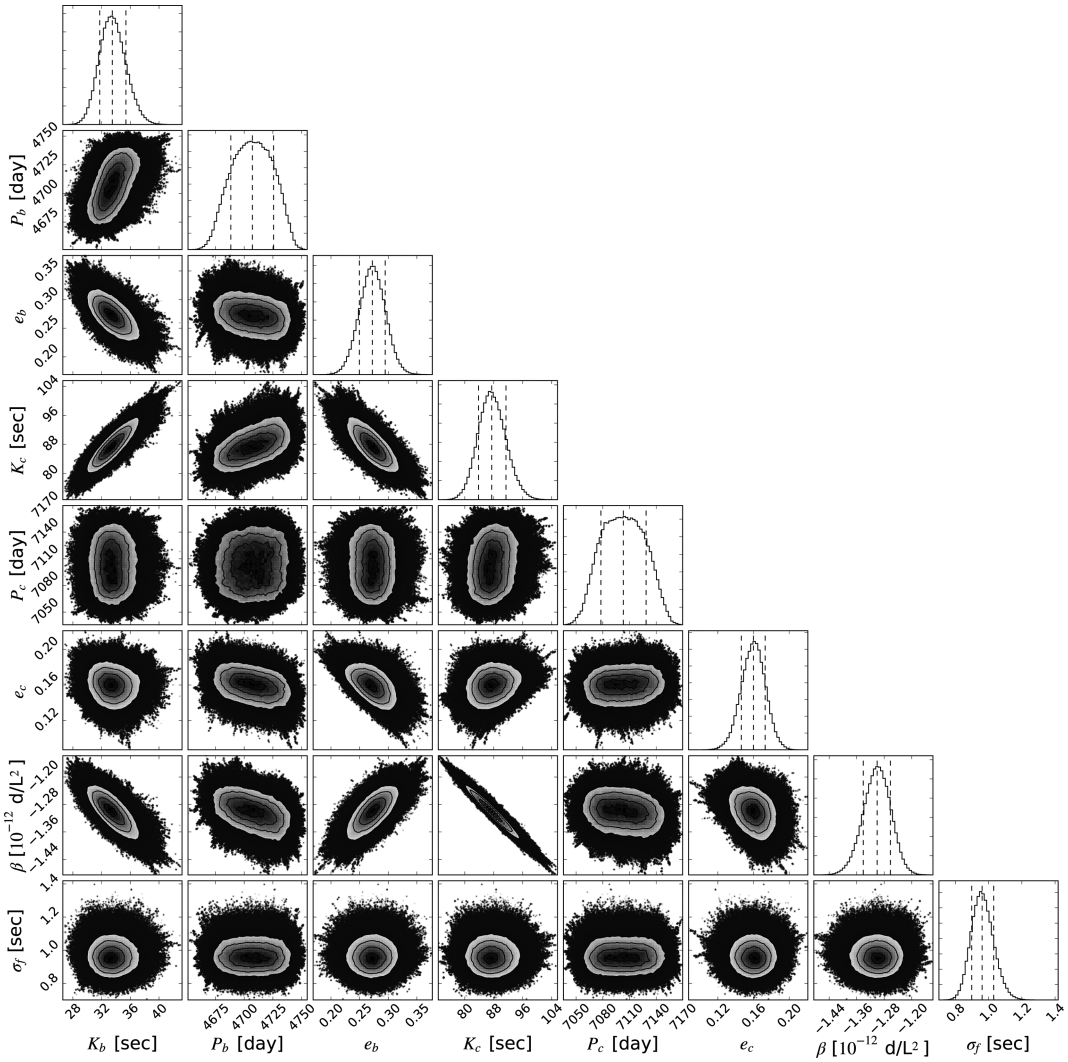

Figure 6. One- and two-dimensional projections of the posterior probability distribution for the best-fitting kinematic model JQ with the parabolic ephemeris, for a few selected parameters (Table 4).

reveals similar orbital periods $P_{\mathrm{b,c}} \sim 8300$ d. Simultaneously, the semi-amplitudes $K_{\mathrm{b,c}}$ may be as large as ∼1 h. Such huge semi-amplitudes imply companion masses in the range characteristic for red dwarfs and massive stars. This is of course non-physical outcome of the mathematical model. The best-fitting solution JL is illustrated in Fig. 7, see Table 4 for its parameters. A particular orientation of orbits with very similar periods, and anti-aligned planets provides the same (O−C) in wide ranges of masses. The same kind of degeneracy of kinematic two-planet model with the linear ephemeris is present in the older data, and we discussed this problem in Goździewski et al. (2012). Looking at the residuals (bottom panel in Fig. 7), we notice systematic, though apparently small deviation from zero at the end of the observing window. All best-fitting models to the linear ephemeris exhibit measurements similarly outlying from their synthetic solutions.

We found that the JL parameter correlations are much stronger than for the quadratic ephemeris. This is illustrated by the projections of the MCMC posterior probability distributions for a few selected model parameters in Fig. 8. A reliable determination of their uncertainties is very difficult unless the model is not re-parametrized in some particular way. The JL solution is quoted solely to show

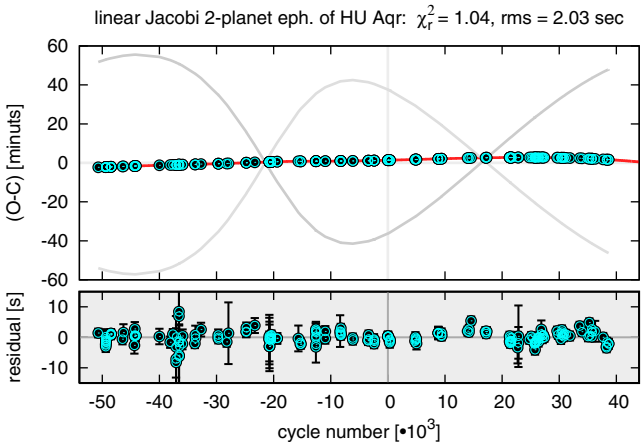

Figure 7. The synthetic curve for the best-fitting two-planet model JL with the linear ephemeris (see Table 4 for its parameters). Shaded curves are for individual signals of both companions, respectively.

Downloaded from http://mnras.oxfordjournals.org/ by guest on February 11, 2015

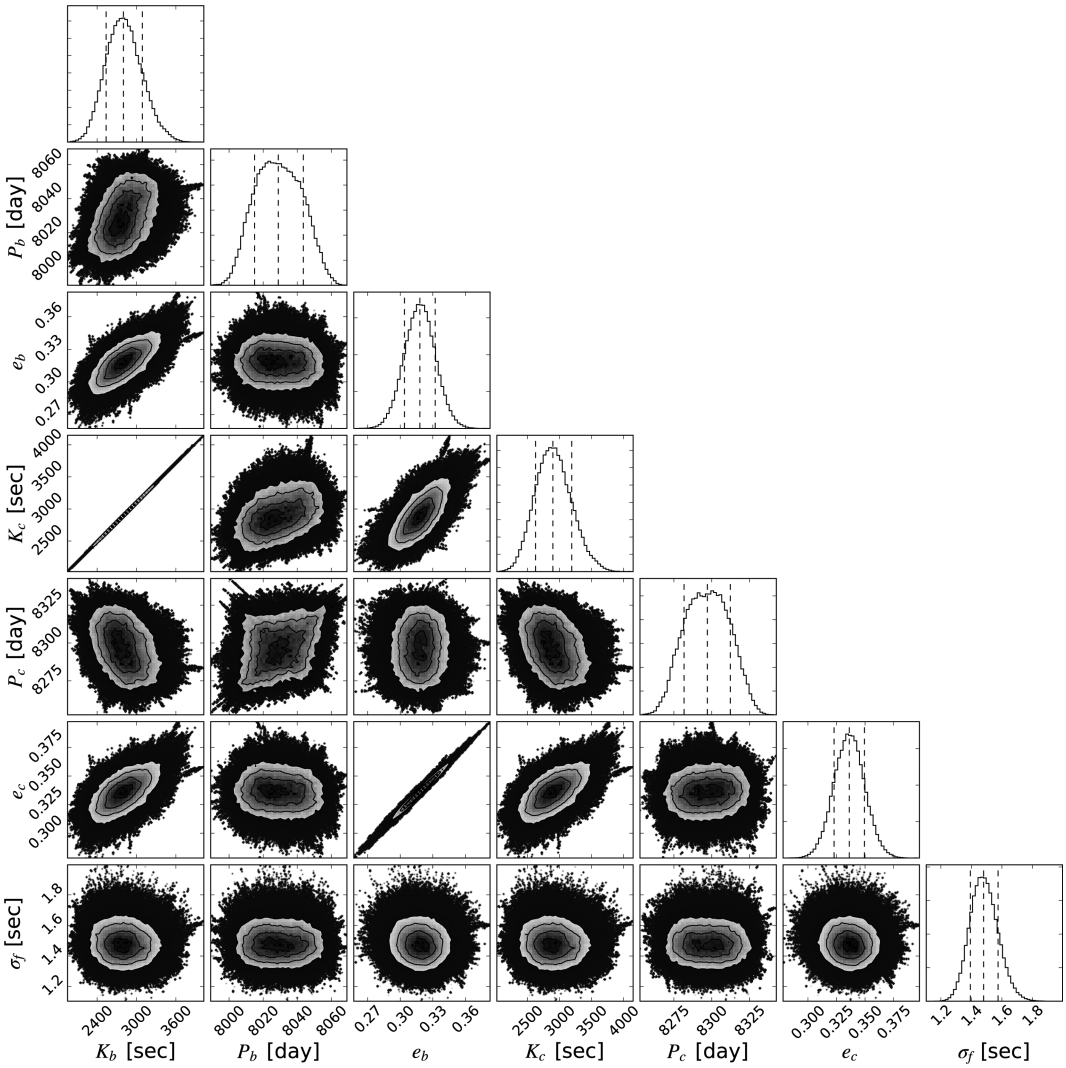

Figure 8. Projections of the MCMC posterior probabilities for selected parameters of the best-fitting solution JL (see Table 4 for elements of this fit). Note extremely large semi-amplitudes of individual LTT signals, strong correlations between similar orbital periods $P_{\mathrm{b,\,c}}$ and between semi-amplitudes $K_{\mathrm{b,\,c}}$.

extreme values of its non-physical parameters and its degenerate character.

3.5 Conversion of Keplerian elements to the *N*-body frame

Following a common approach in the recent literature, we should check whether the best-fitting planetary systems are dynamically stable. Moreover, recalling close orbital periods in the best-fitting solutions JQ and JL, kinematic models may be invalid at all, due to significant mutual gravitational interactions between the planets. This will be shown in the next section.

To accomplish numerical *N*-body integrations, we need to transform the initial conditions from the Jacobian, kinematic frame, to the *N*-body Cartesian coordinates at the osculating epoch T_0[3]. An example of such a conversion for Fit JQ is illustrated in Fig. 5. The right-hand panel shows systematic trends of the residuals to the *N*-body solution outside the T_0 epoch. Indeed, a direct comparison of the synthetic signals derived from the kinematic and *N*-body models differ by ± 10 s (Fig. 9). This might be still considered as a subtle difference, however, the *N*-body osculating initial condition derived from Fit JQ provides $\chi^2_\nu > 7.29$, though $\chi^2_\nu \sim 1$ for the original, source kinematic model. This means that the transformed kinematic initial conditions are poorly consistent with observations. A similar discrepancy of Newtonian and kinematic two-planet models has been shown in Marsh et al. (2014) for the (O−C) of NN Serpentis. These differences for HU Aqr are 10 times larger, likely due to larger planetary masses and smaller separation of orbits. In some parts of this window they may be compared to the signal itself. Recalling a possibility of massive companions, this shows that the LTT signal of HU Aqr cannot be properly modelled even in terms of the Jacobian, refined kinematic formulation.

Fortunately, the gathered huge sets of $\sim 10^6$ Jacobian fits with $\chi^2_\nu < 9$ may be still used as relatively accurate approximations of the proper osculating elements. These solutions were further refined in terms of the exact *N*-body model. Such an approach is helpful for CPU-efficient and quasi-global exploration of the parameter space of the Newtonian models.

[3] Note, that in the literature, kinematic elements derived as 'raw' parameters of the (O−C) model, equation (3), are usually interpreted incorrectly as osculating, *Keplerian, astrocentric* elements w.r.t. the CM of the binary.

Downloaded from http://mnras.oxfordjournals.org/ by guest on February 11, 2015

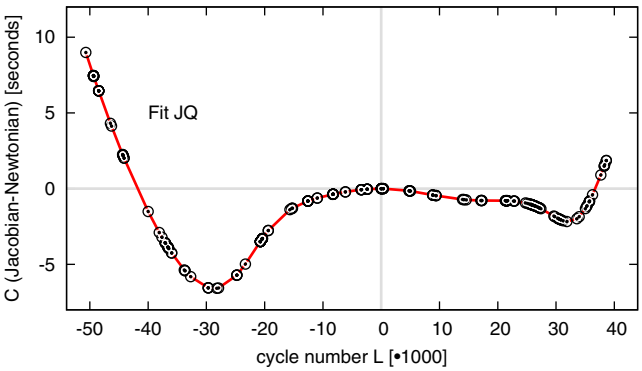

Figure 9. Differences of the LTT signals derived from Jacobian, kinematic solutions JQ (Table 4) and from respective, osculating *N*-body model, integrated numerically with the inferred initial condition at the osculating epoch of the $L = 0$ cycle. The $L = 0$ cycle is centred roughly at the middle of the observational window.

3.6 The *N*-body two-planet model with parabolic term

The refined set of *N*-body models with parabolic ephemeris is illustrated in Fig. 10. Green filled circles in this figure encode solutions $\chi^2_\nu < 1.06$ (roughly 3σ of the best-fitting model NQ1 displayed in Table 5). This distribution of best-fitting solutions is bimodal, with two types of planetary configurations. The first type is close to the best-fitting model NQ1 providing $\chi^2_\nu \sim 0.96$ and characterized by very similar semimajor axes of both companions, $a_{\mathrm{b,c}} \sim 5.7$ au, and with strongly correlated and unconstrained masses, drawn up to $120 m_{\mathrm{Jup}}$. Similar semimajor axes indicate the 1:1 MMR. The second, shallow minimum of $\chi^2_\nu \sim 1.02$ is for solutions around the 3:2 MMR (Fit NQ2), since the semimajor axes are close to ∼5.5 and ∼6.5 au, respectively. These best-fitting models are illustrated in Fig. 11.

The MCMC analysis reveals that though a clear correlation persists between the outermost period and the period derivative term, this correlation is significantly weaker than in the kinematic model. This parameter has a large magnitude of $\beta \simeq -4 \times 10^{-12}$ d L^{-2} and $\beta \simeq -7 \times 10^{-12}$ d L^{-2}, respectively. The MCMC derived posterior probability distribution histograms (not shown here) confirmed in independent way that both solutions, derived and illustrated through the HA projections in Fig. 10, are relatively well bounded in the parameter space, except for a very strong correlation of masses in Fit NQ1, similar to correlation of semi-amplitudes in Fit JL.

We also computed the Newtonian models with the linear ephemeris. In this case, only one minimum of χ^2_ν is apparent in the region of the 1:1 MMR, with both semimajor axes around

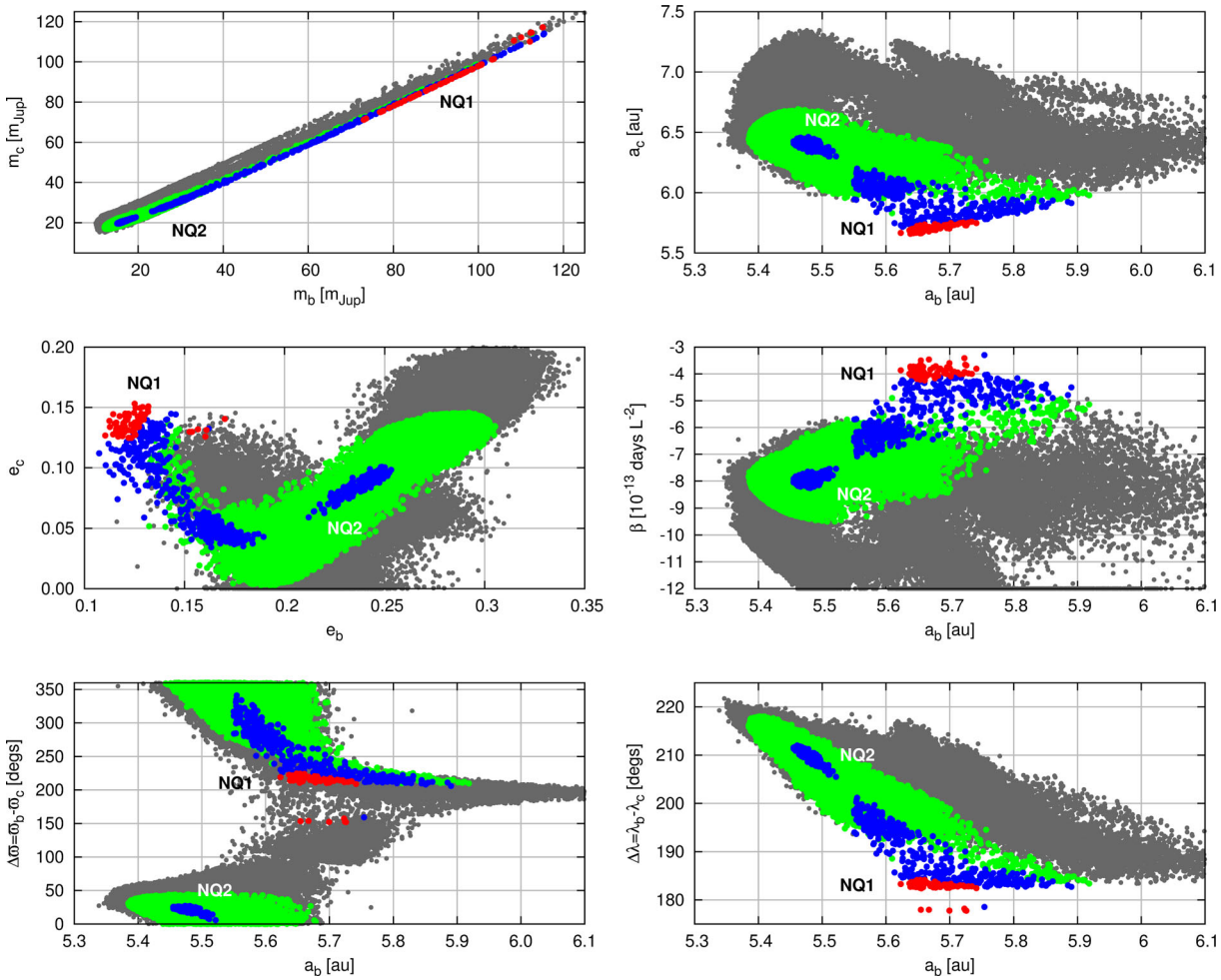

Figure 10. Best-fitting two-planet Newtonian solutions with the quadratic term projected on to planes of orbital elements at the osculating epoch T_0. Red filled circles are for the best-fitting models with $\chi^2_\nu < 0.96$, blue filled circles are for $\chi^2_\nu < 1.02$, green filled circles are for $\chi^2_\nu < 1.06$ (roughly 3σ of Fit NQ1) and grey filled circles are for $\chi^2_\nu < 1.17$, respectively. Solutions NQ1 and NQ2 displayed in Table 5 are labelled.

Downloaded from http://mnras.oxfordjournals.org/ by guest on February 11, 2015

Table 5. Newtonian parameters of two best-fitting two-planet LTT models with parabolic ephemeris, NQ1 and NQ2, respectively. Synthetic curves with mid-egress times are illustrated in Fig. 11. Digits in parentheses are for the uncertainty at the last significant place. Total mass of the binary is 0.98 $M_{\odot}$ (Schwope et al. 2011).

Parameters	Fit NQ1	Fit NQ2
m_b [m_{Jup}]	96.2 ± 9.4	16.8 ± 1.0
a_b (au)	5.68 ± 0.06	5.48 ± 0.06
e_b	0.147 ± 0.015	0.230 ± 0.028
ω_b (deg)	250.8 ± 7.3	92.3 ± 7.5
M_b (deg)	170.3 ± 7.7	115.6 ± 4.1
m_c [m_{Jup}]	98.3 ± 9.5	20.8 ± 1.3
a_c (au)	5.67 ± 0.06	6.38 ± 1.56
e_c	0.123 ± 0.011	0.083 ± 0.027
ω_c (deg)	103.0 ± 8.1	72.6 ± 9.2
M_c (deg)	140.8 ± 9.0	286.5 ± 5.63
P_{bin} (d)	0.086 820 3933(9)	0.086 820 3796(1)
Δt_0 [BJD 2,453,504.0+]	0.888 38(3)	0.888 84(1)
β [$\times 10^{-13}$ d L^{-2}]	−3.7(2)	−7.9(5)
σ_f (s)	0.94(7)	0.94(8)
N_{obs} data points	205	205
N_{par} free parameters	14	14
χ^2_ν	0.96	0.96
rms (s)	1.73	1.78

∼7 au. However, all orbital parameters are spread over wide ranges. There is also a strong correlation between unconstrained companion masses, which reach the non-physical stellar mass range, similar to the kinematic two-planet linear ephemeris. This correlation has the same geometric source as in the Keplerian model, since it appears due to particularly anti-aligned orbits with similar semimajor axes. Therefore, the best-fitting, coplanar two-planet models with the linear ephemeris must be also considered as highly unconstrained and non-physical.

3.7 Stability analysis of two-planet solutions

At a stage of the *N*-body correction of Keplerian models, we verified the dynamical stability of all solutions with final $\chi^2_\nu < 4.0$, by the direct numerical integration of the *N*-body equations of motion with the Bulirsch–Stoer algorithm. To quantify the dynamical stability, we determined the crossing time of orbits (the Event Time, T_E from hereafter) for a time span of $\sim 10^6$ outermost orbital periods. If T_E is shorter than this limiting integration time, then this indicates a close encounter between components or the ejection of a planet from the system. We did not find any stable solutions in the set of $\sim 10^6$ models with the parabolic ephemeris, close to the best-fitting solutions NQ1 and NQ2 (as illustrated in Fig 10), except for just a few hierarchical configurations with $\chi^2_\nu > 1.6$. Such stable solutions are characterized by the outermost semimajor axis $a_c \sim 15$ au and a large mass of the outer companion $\sim 69\, m_{Jup}$, i.e. in a region of the parameter space separated by a few σ from the best-fitting models.

This still does not prove that stable configurations with reasonably small χ^2_ν do not exist in some regions of the parameter space, consistent with observations. For instance, the angular elements of such solutions might be systematically displaced from a stable MMR region (e.g. Goździewski & Maciejewski 2001; Goździewski & Migaszewski 2014). Therefore, to understand the observed instability, we carried out extensive Monte Carlo experiments. For the two-planet quadratic ephemeris solutions, we selected grids of 400 × 400 and 400 × 800 points in the semimajor axes plane (a_b, a_c), spanning $a_b \in [5, 7]$ au, $a_c \in [5, 8]$ au for fit NQ1, and $a_b \in [4.5, 6.5]$ au, $a_c \in [4.5, 9.5]$ au for fit NQ2, respectively. Next, at each point of the given grid, we computed the Mean Exponential Growth factor of Nearby Orbits (MEGNO hereafter) for up to 1 Myr (i.e. up to a few 10^4 outermost orbital periods). MEGNO (Goździewski & Maciejewski 2001; Cincotta, Giordano & Simó 2003) is a numerical algorithm making it possible to estimate efficiently the Maximal Lyapunov Exponent and to determine quasi-regular and chaotic solutions of the *N*-body equations of motion. In the examined ranges of semimajor axes, two-planet systems may be stable only in the regime of MMRs, and chaotic solutions imply short-time geometric instability (hence short T_E) (e.g. Goździewski & Migaszewski 2014).

The MEGNO indicator was computed 2880 times at each point of a particular (a_b, a_c)-grid: at each point of this grid, the argument of pericentre $\varpi_c \in [0^\circ, 360^\circ]$ was gradually increased from 0° to 360° by $\Delta\varpi_c = 0^\circ.125$, and for a such a particular value of ϖ_c, we selected random eccentricities within $[0, e_{b,c} + 0.2)$ around a given best-fitting solution, and random mean anomaly $M_c \in [0^\circ, 360^\circ]$. In this way, we obtain an extensive and exhaustive mapping of the multidimensional parameter space. The tested sets of initial conditions for the best-fitting models NQ1 and NQ2 contain of $\sim 4 \times 10^8$ and $\sim 9 \times 10^8$ elements, respectively. (Note that planetary

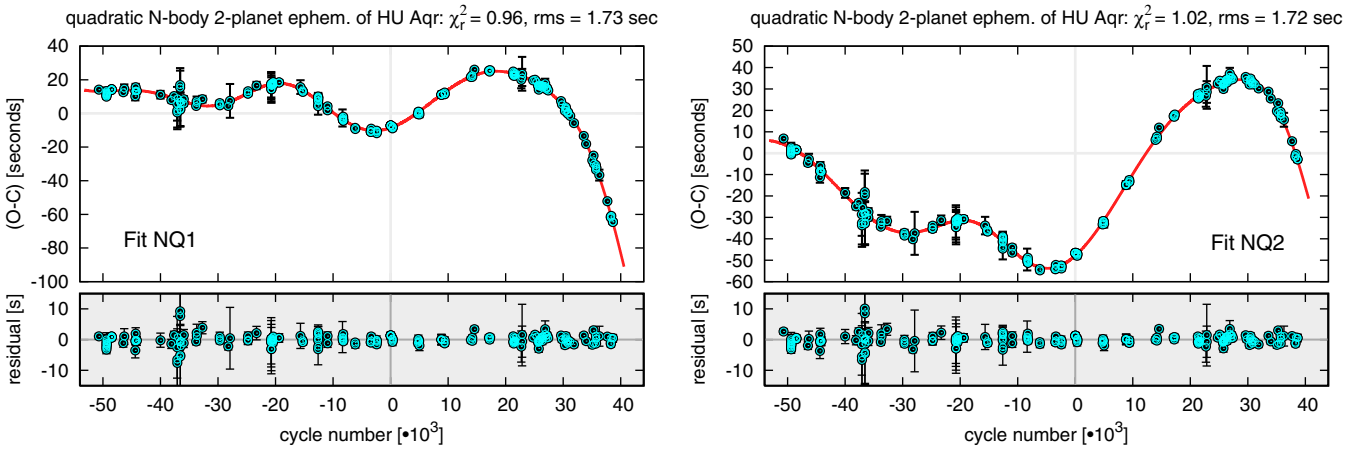

Figure 11. Best-fitting Newtonian two-planet quadratic ephemeris models: Fit NQ1, left-hand panel, and Fit NQ2, right-hand panel, respectively. See Table 5 for parameters of these solutions.

Downloaded from http://mnras.oxfordjournals.org/ by guest on February 11, 2015

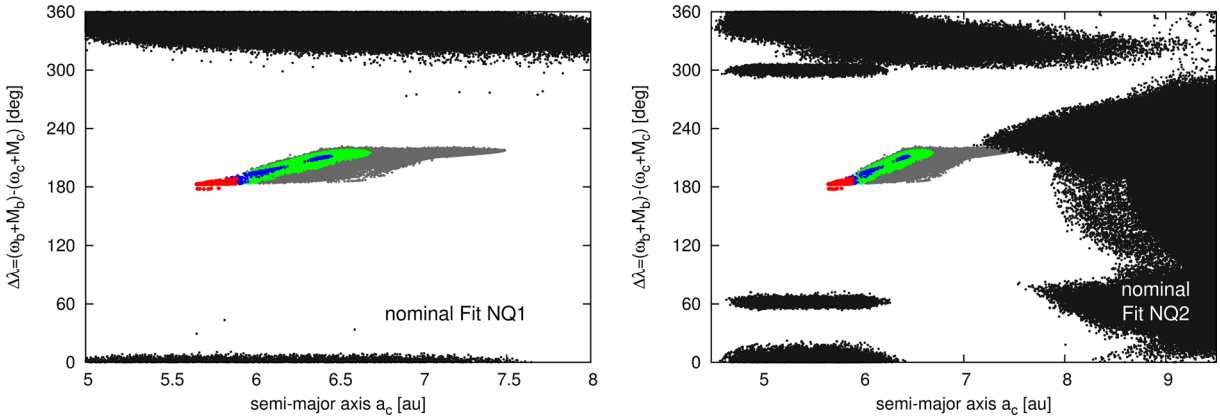

Figure 12. Illustration of stability analysis of the two-planet Newtonian models NQ1 (left-hand panel), and NQ2 (right-hand panel) in the ($a_{\rm b,\,c}$, $\Delta\lambda$)-planes, where $\Delta\lambda$ is the initial difference between the mean longitudes of the planets. Dark grey points are for stable initial conditions, light grey and coloured points are for models within $\chi^2_\nu < 1.21$ (a few σ-confidence levels of the best-fitting model NQ1). White colour is for unstable configurations. See the text for details.

masses were kept fixed in both tests at their nominal values of NQ1 and NQ2 solutions in Table 5.) Then we computed MEGNO for each initial conditions and gathered all regular (quasi-periodic) models. Such massive computations would be hardly possible to conduct without a help of our Message Passing Interface (MPI) code μFARM run at the `cane` computer cluster (Poznań Supercomputing Centre PCSS, Poland).

The results are illustrated in two panels of Fig. 12, in the ($a_{\rm b,\,c}$, $\lambda_{\rm b} - \lambda_{\rm c}$)-planes around initial orbital elements corresponding to Fits NQ1 and NQ2, respectively. For reference, we overplotted the statistics of the best-fitting solutions (Fig. 10). White regions in this figure mean that *any tested combination* of the orbital elements, even not necessarily consistent with the observed (O−C), has a positive Lyapunov Exponent (therefore is unstable). The best-fitting models are found around initial $\Delta\lambda_{\rm b,\,c} = \lambda_{\rm b} - \lambda_{\rm c} \sim 180^\circ$, hence in antiphase with possible stable models (dark, grey filled circles in Fig. 12). Both these regions are completely separated up to $\chi^2_\nu \sim 1.17$, more than a few σ levels. This suggests that stable configurations are unlikely within the parameter ranges permitted by the observations, recalling the huge volume of initial conditions examined in both experiments. Similar Monte Carlo tests were repeated a few times more for different nominal best-fitting models obtained on the basis or earlier observations, and also their results are negative. We note that stable configurations with proper $\Delta\lambda$ are possible for systems with the outermost semimajor axis $a_{\rm c}$ greater than ∼15 au. However, such models are poorly consistent with the observations, implying $\chi^2_\nu > 1.56$, as described above.

A similar stability test for the two-planet *N*-body linear ephemeris, has only a formal sense, due to the large and unconstrained masses of the planets. We selected a solution with semimajor axes ∼7 au and relatively small masses of the planets, ∼120 $m_{\rm Jup}$, still unlikely in the real HU Aqr system. Similar to the previous experiment, stable models exhibit $\Delta\lambda$ in antiphase with the gathered statistics of the best-fitting models. Stable systems with both semimajor axes ∼7 au (close to the 1:1 MMR) are possible only when both planets are roughly aligned in their orbits with *anti-aligned* apsidal lines, similar to the parabolic case (see the left-hand panel in Fig. 12) and may persist even in extreme mass ranges. Therefore, such apparently unlikely 1:1 MMR configurations *should not be*a priori considered as dynamically unstable.

3.8 Three-planet models with the linear ephemeris

The best-fitting two-planet solutions NQ1 and NQ2 exhibit excessively large period derivative $\beta \sim -10^{-12}{\rm d}\,L^{-2}$, which may be interpreted as the LTT delay induced by a third companion with a very long orbital period. This period may be estimated by the curvature of the parabolic trend of the (O−C), compared to the observational window ∼20 yr. Since only a small fraction of the orbit is apparent, the orbital period would be multiplied by a factor of 2–3 or larger.

If to allow for a hypothesis of such a highly hierarchical three-planet configuration, we may focus first on the innermost two-planet close-in systems. In Goździewski et al. (2012), we found stable two-planet configurations in a region of moderate eccentricities. However, similar to the HW Vir case (Beuermann et al. 2012), the outermost orbit of these models is not well determined. The present data of HU Aqr, extending the observational window by only ∼10 per cent, seem to narrow possible solutions to a much more compact set overlapping with the previously derived 3:2 MMR configurations. In the current models, both semimajor axes are simultaneously shifted by ∼1 au to a secondary region of unstable models in the ($a_{\rm b}$, $a_{\rm c}$)-plane in Goździewski et al. (2012, see their fig. A3, *left-bottom* panel). Moreover, the best-fitting *N*-body configuration corresponds to the 1:1 MMR with very similar orbital periods and masses, reaching the non-physical region of two red dwarf companions. This solution is robust, and is preserved with the up-to date mid-egress timing. The change of the orbital parameters is caused by the fast decay of the (O−C) over past 2 years. We did not find any *stable, coplanar two-planet* strictly consistent with observations; however, such systems might be stable if the planets were placed initially in antiphase with their actual, predicted 'observational' positions. It may be understood as a strong, dynamical indication of plainly inadequate or incomplete LTT model of the low-period component of the (O−C).

Therefore, we performed the *N*-body search in terms of the three-planet linear ephemeris model, at first with planets in coplanar and direct orbits. As the result, we obtain that basically any combination of masses up to the red dwarf mass limit, semimajor axes in the range up to 20 au, and eccentricities ∈ [0, 1) are possible, still providing $\chi^2_\nu \sim 1$. A typical semimajor axis of the outermost planet in these three-planet models is larger than 16 au. We also did not

Downloaded from http://mnras.oxfordjournals.org/ by guest on February 11, 2015

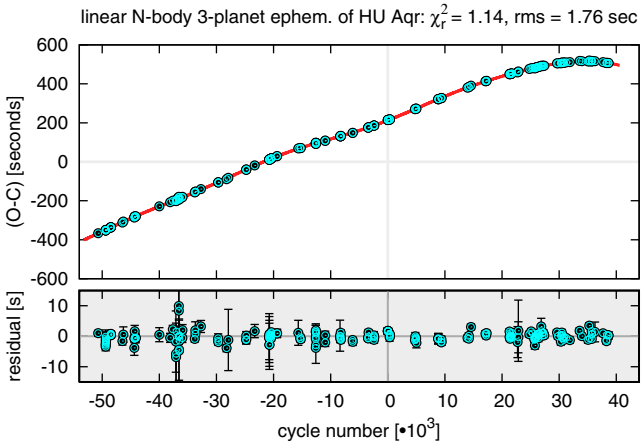

Figure 13. Synthetic curve of dynamically stable three-planet model with the linear ephemeris (NL3). The osculating, astrocentric orbital elements at the epoch of T_0 =BJD 245 3504.888 2940, expressed by tuples (m – mass [$m_{\rm Jup}$], a – semimajor axis [au], e – eccentricity, i – inclination [deg], Ω – node [deg], ω – argument of pericentre [deg], M – mean anomaly [deg]) for each planet are: (4.758 $m_{\rm Jup}$, 3.602 au, 0.0218, 90°, 0°, 173°.01, 133°.69), (20.20 $m_{\rm Jup}$, 6.557 au, 0.1365, 90°, 180°, 10°.77, 245°.50), (80.00 $m_{\rm Jup}$, 12.887 au, 0.0158, 90°, 0°, 311°.94, 83°.47), for planets b, c and d, respectively. The initial epoch of the ephemeris t_0 = BJD 2453504888294, $P_{\rm bin}$ = 0.086 820 2747 d. Total mass of the binary is 0.98 M$_\odot$. This model provides $\chi^2_\nu \simeq 1.14$ and an rms $\simeq$ 1.76 s with 205 data points and 17 free parameters (inclinations and nodes are fixed). The error correction is $\sigma_{\rm f}$ = 0.9 s. Formal uncertainties of the NL3 solution are difficult to estimate, since this model is displaced from the minimum of $\chi^2_\nu \sim 0.9$ and an rms ~1.71 s and is localized in dynamically complex zone.

find any stable models with coplanar and direct orbits providing $\chi^2_\nu < 3.3$, through setting different constraints for these models (moderate eccentricities, circular orbit of the outermost component, hierarchical configuration of the planets).

The assumption of coplanar systems with all direct orbits still does not preclude stable *spatial* two- or three-planet configurations, with high mutual inclinations, up to the limit of coplanar counter-rotating companions. In the most extreme case, such systems tend to be much more stable than configurations with the direct orbits (Eberle & Cuntz 2010; Morais & Giuppone 2012; Goździewski et al. 2013). Strongly resonant systems may be also possible, with three planets involved in deep, low-order and very narrow MMRs, like in the HR 8799 planetary system exhibiting Laplace 4:2:1 MMRs (Goździewski & Migaszewski 2014) confined to small stable islands in the semimajor axes–eccentricity space.

As an illustration, we show here an example of a stable three-planet model with the linear ephemeris (NL3, see Fig. 13), which was found through the HA, permitting that one of the planets is in *retrograde* orbit with respect to two remaining planets in *prograde* orbits. This solution, providing $\chi^2_\nu \sim 1.14$ and very small rms 1.76 s (similar to the best-fitting two-planet solutions), belongs to a family of stable, small-eccentricity orbits with semimajor axes of ~3.6, ~6.6 and ~13 au, respectively. Moreover, the outermost planet's mass is heavily unconstrained and may be as large as 80 $m_{\rm Jup}$.

In spite that the innermost and the middle planets' are also massive (~5 $m_{\rm Jup}$ and ~16 $m_{\rm Jup}$, respectively), and the system is dynamically packed, it remains stable for at least 1 Gyr. The evolution of bounded semimajor axes for such an interval of time is shown in Fig. 14. To show the dynamical neighbourhood of this particular model, we computed the MEGNO dynamical map, varying the semimajor axis and eccentricity of the middle planet, and keeping other parameter fixed at its nominal values. The dynamical map (Fig. 15) reveals that this model (and the whole family of solutions of this class) is localized in a relatively extended stable zone, spanned by a dense net of two-body and three-body MMRs. As a 'side-effect' of this experiment, we detected the so-called Arnold web, seen as weak, vertical 'X'-like structures in Fig. 15. The Arnold web emerges due to overlapping unstable MMRs and their branches (e.g. Goździewski et al. 2013) in strongly perturbed planetary systems.

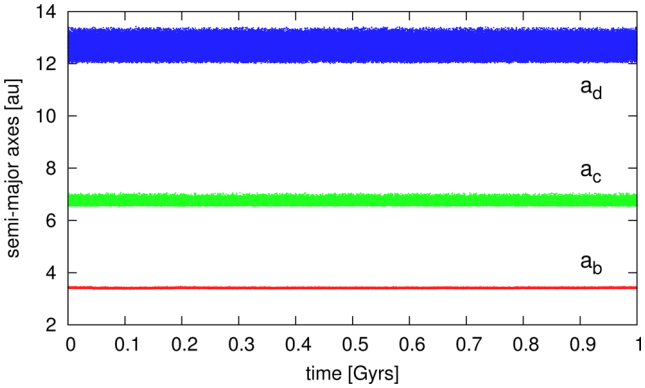

Figure 14. Evolution of semimajor axes in the long-term stable model NL3 with the middle planet in a retrograde orbit. Osculating elements of this model are displayed in caption to Fig. 14.

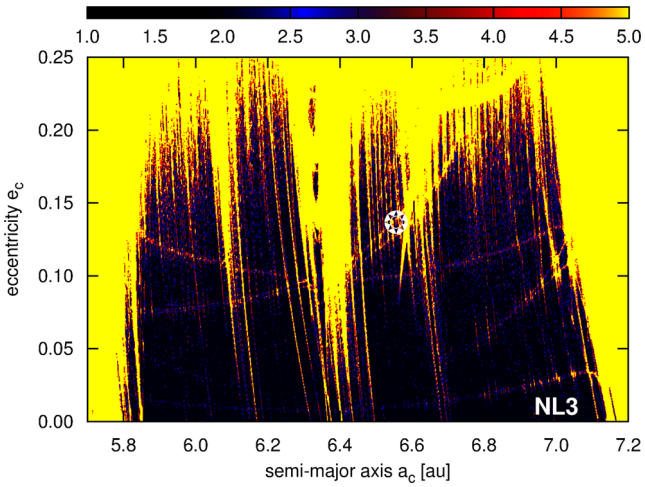

Figure 15. A dynamical map in terms of the MEGNO indicator for the long-term stable model NL3 in the (semimajor axis a_c, eccentricity e_c)-plane of the middle planet. The nominal model is marked with the star symbol. The dynamical stability is colour-coded: dark blue (black) with MEGNO ~2 is for quasi-periodic configurations, yellow (grey) is for chaotic, strongly unstable models. The resolution of the map is 1024 × 768 initial conditions. Each configuration was integrated for 1.6 Myr (50 000 outermost periods). See the text for details.

This NL3 solution is peculiar, because the middle orbit is retrograde (the orbital spin vector is antiparallel to the orbital spins of two remaining companions). We constrained the NL3 model by restricting the absolute inclinations to one plane and fixing nodal lines, since this minimizes the number of free-parameters required to describe the spatial model. Releasing these constraints, we also found stable solutions with mutual inclinations reaching 180°, which result in reasonably small rms of ~1.8 s. Such apparently extreme solutions should not be necessarily excluded as non-physical and non-realistic. The dynamical environment of the putative planetary system has strongly changed during the common envelope phase

Downloaded from http://mnras.oxfordjournals.org/ by guest on February 11, 2015

(Portegies Zwart 2013). This might force a dynamical instability of the system and close encounters which resulted in highly inclined orbits.

4 DISCUSSION AND CONCLUSIONS

The HU Aqr binary belongs to the class of evolved binaries after the post-common envelope phase or compact binaries, which presumably host single or multiple planetary companions (e.g. Beuermann et al. 2010, 2011; Qian et al. 2010; Yang et al. 2010; Potter et al. 2011; Lee et al. 2012; Almeida, Jablonski & Rodrigues 2013; Lee, Hinse & Park 2013; Marsh et al. 2014). These papers claim (explicitly, or implicitly) that the observed (O−C) variability can be explained by the Rømer effect. Circumbinary planets exist, indeed, since they have been recently detected and confirmed independently through photometry of the KEPLER telescope (e.g. Orosz et al. 2012; Welsh et al. 2012, 2014).

However, the LTT hypothesis suffers from ambiquities regarding optimization methods, dynamical models of putative planetary systems, as well as phenomena intrinsic to the binaries.

Recent studies of multiple-planet systems detected by the (O−C) technique revealed that their orbits are close to low-order MMRs and strongly unstable, for time-scales as short as thousands of years (e.g. Horner et al. 2012, 2013; Lee, Hinse & Park 2013; Wittenmyer, Horner & Marshall 2013; Hinse, Horner & Wittenmyer 2014; Lee et al. 2014). The only well-documented exception seems to be the NN Ser system (Beuermann et al. 2010; Marsh et al. 2014) which presumably hosts a long-term stable system of two Jovian planets involved in the 2:1 MMR or the 5:2 MMR. Also the two-planet HW Vir system (Lee et al. 2009; Beuermann et al. 2012) may be resonant and stable, though the semimajor axis of the outer planet, and its mass are yet not well determined. HU Aqr is perhaps one of the most enigmatic members of this class of putative planetary systems. Its analysis provides interesting clues, spanning observational aspects, through the proper modelling of the (O−C), the dynamical evolution and stability and possible scenarios of their formation (e.g. Portegies Zwart 2013).

In this work, we tested the LTT effect, which may be present in the HU Aqr, on strict dynamical grounds. In the very recent paper, Bours et al. (2014) conclude that the (O−C) derived two-planet and three-planet systems around this binary are unstable due to large eccentricities. We found that such coplanar configurations are unstable due to semimajor axes in similar ranges and large and unconstrained planetary masses reaching the non-physical range of red dwarfs, and particular relative phasing on the planets in their orbits. Actually, the best-fitting models exhibit small and moderate eccentricities. They are degenerated due to strong correlations between their physical and geometrical parameters.

The HU Aqr data provide a clear example that the Keplerian and *N*-body formulations of the LTT effect for multiple planetary systems may lead to qualitatively different views on its parameter space. Observational windows of the binaries are narrow relative to the putative orbital periods, and the inferred masses of hypothetical planets are large, up to the brown dwarf and the red dwarf limits, like in the SZ Her system (Hinse et al. 2012a). In such settings, the conversion of model parameters between both reference frames may introduce significant deviations between synthetic signals derived from the Keplerian, and osculating Newtonian elements. This may qualitatively modify the statistics of best-fitting configurations constrained by the available data. Moreover, the LTT models of HU Aqr suffer from strong correlations between different parameters, which makes the problem of reliable optimization of these models even more complex. Similar correlations are reported by Marsh et al. (2014) for the parabolic ephemeris of NN Ser.

Our results indicate that the LTT hypothesis for the eclipse timing of HU Aqr is uncertain. Recalling the geometric source of the instability of coplanar two-planet configurations, more elaborate dynamical models to describe the observed (O−C) are required, like the three-planet model with large relative inclinations, as described above.

Moreover, the results in Lanza et al. (1998) and Lanza (2006) still support the quadrupole moment variations as the source of the (O−C), though the Applegate effect is usually dismissed in the literature. To show this, we extrapolated formulae in Wang et al. (2010, their equation 7) for the luminosity variation $\Delta L/L$ of the secondary component M4V, as derived for the modified Applegate mechanism in Lanza et al. (1998) and Lanza (2006) and references therein. We found that $\Delta L/L \sim 8 \times 10^{-6}$ in the relative units, adopting the radius $R = 0.22\,\mathrm{R}_\odot$, mass $M = 0.18\,\mathrm{M}_\odot$, orbital separation $a = 0.0032$ au, and the effective temperature $T = 3400$ K of the secondary. Indeed, in accord with Lanza et al. (1998), the luminosity variations associated with the Applegate mechanism should be effectively smoothed out, given the much longer thermal time-scale of the stellar convection zone and they may be hardly observable. We also estimated the quadrupole period variation ΔQ needed to drive the modulation of the orbital period (Lanza & Rodonò 1999)

$$\frac{\Delta P_{\rm bin}}{P_{\rm bin}} = -9\frac{\Delta Q}{Ma^2} \equiv \frac{4\pi K}{P_{\rm mod}},$$

where we adopted the semi-amplitudes $K_{\rm b,\,c}$ and the orbital periods $P_{\rm b,\,c}$ in Fit JQ (Table 4) as estimates for the semi-amplitude K of the orbital period modulations, and for the modulation period $P_{\rm mod}$, respectively. We obtain $\Delta P_{\rm bin}/P_{\rm bin} \sim 10^{-6}$, $\Delta Q \sim 1 \times 10^{47}$ g cm^2 and $\sim 2 \times 10^{47}$ g cm^2, respectively, which are in the range characteristic for other short-period CVs systems (Lanza & Rodonò 1999). The order of magnitude of these variations of $\sim 5 \times 10^{47}$ g cm^2 is typical for a possible Applegate-like mechanism (Lanza, private communication). Therefore, this mechanism leaves the LTT effect only as a reasonable possibility among other explanations of the (O−C).

We certainly need an independent observational approach to shed more light on this problem. Such a technique might be the astrometric monitoring of the binary. HU Aqr is a relatively distant object at ∼200 pc. However, provided the accuracy of ∼30 μs which is accessible by the ongoing *GAIA* mission, a detection of its putative companions may be possible after 5 yr observations. A simulation of the astrometric signal of a single-planet system with a 7 Jovian mass planet in a 5 au orbit (Fig. 16) reveals its amplitude of ∼0.3 mas. If the putative outermost, massive companion is very distant from the binary, as it might be suggested by the β term, then already well-developed direct imaging technique might confirm its presence directly. Combined with a proper dynamical model, such a detection might at least put some constraint on its mass and orbital distance (Goździewski & Migaszewski 2014).

The results of our paper preclude the hypothesis of any coplanar two-planet system around HU Aqr. A three-planet system with one planet in a retrograde orbit or with high mutual inclinations might be possible, but its reliable detection on the basis of the (O−C) data is unlikely too, recalling the short time-span of the observations. It is also possible that the intrinsic binary's activity and the quadrupole modulations of the secondary due to magnetic cycles may be fully responsible for the observed (O−C) signal or for its significant fraction, similar to stellar spots which 'pollute' the RV and transit data (e.g. Montalto et al. 2014). We postpone the analysis of such

Downloaded from http://mnras.oxfordjournals.org/ by guest on February 11, 2015

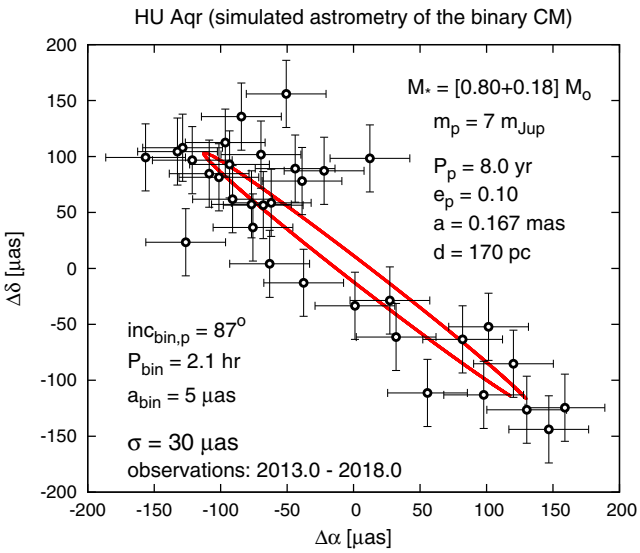

Figure 16. A simulation of the astrometric reflex motion of the mass centre (red ellipse) of the HU Aqr (CM) due to the presence of a circumbinary 7 Jupiter mass planet at 8 years orbit, coplanar with the binary orbital plane ($i = 87°$). The reflex semimajor axis a of the CM is ∼0.17 mas. Accurate observations with the mean uncertainty at 30–50 μas level (open circles with crossed error bars), and spanning about of 5 yr may be sufficient to detect the third-body object.

more complex models of the (O−C) to future papers. The target should be systematically monitored on a long-term time baseline to reveal the true nature of the observed eclipse timing variability.

ACKNOWLEDGEMENTS

We thank the anonymous referee for thorough reviews, critical comments and numerous, constructive suggestions that greatly improved this paper, and in particular, for bringing the Lanza et al. modification of the Applegate mechanism to our attention. We are very grateful to Antonino F. Lanza for explanations regarding the Applegate effect and its observational constraints. This work has been supported by Polish National Science Centre MAESTRO grant DEC-2012/06/A/ST9/00276 (KG), SONATA grant DEC-2011/03/D/ST9/00656 (AS, KK, MŻ) and SONATA BIS DEC-2011/01/D/ST9/00735 (MG). We thank the SKO for their support and allocation of telescope time. SKO is a collaborative project of the University of Crete, the Foundation for Research and Technology Hellas, and the Max-Planck-Institute for Extraterrestrial Physics. This work is based on observations made with the 2 m telescope operated by the NAO in Rozhen (Bulgaria). We thank the staff of NAO for their generous support and telescope time. This work has made use of data obtained at the Thai National Observatory on Doi Inthanon, operated by NARIT. We also provide observations with the 1.55 m Carlos Sánchez Telescope operated on the island of Tenerife by the Instituto de Astrofísica de Canarias in the Spanish Observatorio del Teide. We would like to thank Yucel Kilic for his help with observations at the TÜBİTAK National Observatory. KG thanks the Poznań Supercomputer and Network Centre (PCSS, Poland) for computational grant no. 195 and technical support. Computations in this work were carried out on the `cane` and `chimera` supercomputers of the PCSS. This research has made use of the SIMBAD data base, operated at CDS, Strasbourg, France, and of NASA's Astrophysics Data System Bibliographic Services.

REFERENCES

Almeida L. A., Jablonski F., Rodrigues C. V., 2013, ApJ, 766, 11
Applegate J. H., 1992, ApJ, 385, 621
Baluev R. V., 2008, Celest. Mech. Dyn. Astron., 102, 297
Beuermann K. et al., 2010, A&A, 521, L60
Beuermann K. et al., 2011, A&A, 526, A53
Beuermann K., Dreizler S., Hessman F. V., Deller J., 2012, A&A, 543, A138
Bevington P. R., Robinson D. K., 2003, Data Reduction and Error Analysis for the Physical Sciences. McGraw-Hill, New York
Bours M. C. P. et al., 2014, MNRAS, 445, 1924
Brinkworth C. S., Marsh T. R., Dhillon V. S., Knigge C., 2006, MNRAS, 365, 287
Butler R. P., Marcy G. W., Vogt S. S., Fischer D. A., Henry G. W., Laughlin G., Wright J. T., 2003, ApJ, 582, 455
Charbonneau P., 1995, A&AS, 101, 309
Cincotta P. M., Giordano C. M., Simó C., 2003, Phys. D Nonlinear Phenom., 182, 151
Dhillon V. S. et al., 2014, MNRAS, 444, 3504
Eastman J., Siverd R., Gaudi B. S., 2010, PASP, 122, 935
Eberle J., Cuntz M., 2010, ApJ, 721, L168
Foreman-Mackey D., Hogg D. W., Lang D., Goodman J., 2013, PASP, 125, 306
Goodman J., Weare J., 2010, Commun. Appl. Math. Comput. Sci., 1, 65
Goździewski K., Maciejewski A. J., 2001, ApJ, 563, L81
Goździewski K., Migaszewski C., 2014, MNRAS, 440, 3140
Goździewski K. et al., 2012, MNRAS, 425, 930
Goździewski K., Słonina M., Migaszewski C., Rozenkiewicz A., 2013, MNRAS, 430, 533
Gregory P. C., 2005, ApJ, 631, 1198
Hilditch R. W., 2001, An Introduction to Close Binary Stars. Cambridge Univ. Press, Cambridge
Hinse T. C., Goździewski K., Lee J. W., Haghighipour N., Lee C.-U., 2012a, AJ, 144, 34
Hinse T. C., Lee J. W., Goździewski K., Haghighipour N., Lee C.-U., Scullion E. M., 2012b, MNRAS, 420, 3609
Hinse T. C., Horner J., Wittenmyer R. A., 2014, J. Astron. Space Sci., 31, 187
Horner J., Marshall J. P., Wittenmyer R. A., Tinney C. G., 2011, MNRAS, 416, L11
Horner J., Hinse T. C., Wittenmyer R. A., Marshall J. P., Tinney C. G., 2012, MNRAS, 427, 2812
Horner J., Wittenmyer R. A., Hinse T. C., Marshall J. P., Mustill A. J., Tinney C. G., 2013, MNRAS, 435, 2033
Irwin J. B., 1952, ApJ, 116, 211
Kanbach G., Straubmeier C., Spruit H. C., Belloni T., 2001, Nature, 414, 180
Kanbach G., Stefanescu A., Duscha S., Mühlegger M., Schrey F., Steinle H., Słowikowska A., Spruit H., 2008 in Phelan D., Ryan O., Shearer A., eds, Astrophysics and Space Science Library, Vol. 351, OPTIMA: A High Time Resolution Optical Photo-Polarimeter. Springer-Verlag, Berlin, p. 153
Lanza A. F., 2005, MNRAS, 364, 238
Lanza A. F., 2006, MNRAS, 369, 1773
Lanza A. F., Rodonò M., 1999, A&A, 349, 887
Lanza A. F., Rodonò M., 2002, Astron. Nachr., 323, 424
Lanza A. F., Rodonò M., 2004, Astron. Nachr., 325, 393
Lanza A. F., Rodono M., Rosner R., 1998, MNRAS, 296, 893
Laughlin G., Chambers J. E., 2001, ApJ, 551, L109
Lee J. W., Kim S.-L., Kim C.-H., Koch R. H., Lee C.-U., Kim H.-I., Park J.-H., 2009, AJ, 137, 3181
Lee J. W., Lee C.-U., Kim S.-L., Kim H.-I., Park J.-H., 2012, AJ, 143, 34
Lee J. W., Hinse T. C., Park J.-H., 2013, AJ, 145, 100
Lee J. W., Hinse T. C., Youn J.-H., Han W., 2014, MNRAS, 445, 2331

Downloaded from http://mnras.oxfordjournals.org/ by guest on February 11, 2015

Marsh T. R. et al., 2014, MNRAS, 437, 475
Montalto M., Boué G., Oshagh M., Boisse I., Bruno G., Santos N. C., 2014, MNRAS, 444, 1721
Morais M. H. M., Giuppone C. A., 2012, MNRAS, 424, 52
Nasiroglu I., Słowikowska A., Kanbach G., Haberl F., 2012, MNRAS, 420, 3350
Oscoz A. et al., 2008 in McLean I. S., Casali Mark M., eds, Proc. SPIE Conf. Ser. Vol. 7014, Ground-based and Airborne Instrumentation for Astronomy II. SPIE, Bellingham, p. 701447
Orosz J. A. et al. 2012, Science, 337, 1511
Parsons S. G. et al., 2014, MNRAS, 438, L91
Portegies Zwart S., 2013, MNRAS, 429, L45
Potter S. B. et al., 2011, MNRAS, 416, 2202
Qian S.-B., Liao W.-P., Zhu L.-Y., Dai Z.-B., 2010, ApJ, 708, L66
Qian S.-B. et al., 2011, MNRAS, 414, L16
Richichi A., Irawati P., Soonthornthum B., Dhillon V. S., Marsh T. R., 2014, AJ, 148, 100
Schwarz R., Schwope A. D., Vogel J., Dhillon V. S., Marsh T. R., Copperwheat C., Littlefair S. P., Kanbach G., 2009, A&A, 496, 833
Schwope A. D., Thinius B. D., 2014, Astron. Nachr., 335, 357
Schwope A. D., Thomas H.-C., Beuermann K., 1993, A&A, 271, L25
Schwope A. D., Schwarz R., Sirk M., Howell S. B., 2001, A&A, 375, 419
Schwope A. D., Horne K., Steeghs D., Still M., 2011, A&A, 531, A34
Słowikowska A., Kanbach G., Kramer M., Stefanescu A., 2009, MNRAS, 397, 103
Słowikowska A., Goździewski K., Nasiroglu I., Kanbach G., Rau A., Krzeszowski K., 2013, in Krzesiński J., Stachowski G., Moskalik P., Bajan K., eds, ASP Conf. Ser. Vol. 469, 18th European White Dwarf Workshop. Astron. Soc. Pac., San Francisco, p. 363
Stefanescu A., 2011, PhD thesis, Technische Universität München
Stefanescu A., Kanbach G., Słowikowska A., Greiner J., McBreen S., Sala G., 2008, Nature, 455, 503
Straubmeier C., Kanbach G., Schrey F., 2001, Exp. Astron., 11, 157
Tovmassian G. H., Zharikov S. V., Neustroev V. V., 2007, ApJ, 655, 466
Vogel J., Schwope A., Schwarz R., Kanbach G., Dhillon V. S., Marsh T. R., 2008, in Phelan D., Ryan O., Shearer A., eds, AIP Conf. Proc. Vol. 984, High Time Resolution Astrophysics: The Universe at Sub-Second Timescales. Am. Inst. Phys., New York, p. 264
Wang X.-L., Xiang F.-Y., Tian Y.-P., Shi X.-M., 2010, PASJ, 62, 671
Warner B., 1995, Cambridge Astrophysics Series, 28: Cataclysmic Variable Stars. Cambridge Univ. Press, Cambridge
Welsh W. F. et al., 2012, Nature, 481, 475
Welsh W. F., Orosz J. A., Carter J. A., Fabrycky D. C., 2014, in Haghighipour N., ed., Proc. IAU Symp. 293, Formation, Detection, and Characterization of Extrasolar Habitable Planets. Cambridge Univ. Press, Cambridge, p. 125
Wittenmyer R. A., Horner J., Marshall J. P., Butters O. W., Tinney C. G., 2012, MNRAS, 419, 3258
Wittenmyer R. A., Horner J., Marshall J. P., 2013, MNRAS, 431, 2150
Wright J. T., 2005, PASP, 117, 657
Yang Y.-G., Li H.-L., Dai H.-F., Zhang L.-Y., 2010, AJ, 140, 1687

APPENDIX A: MID-EGRESS TIMES OF HU AQR

Table A1 in this appendix collects mid-egress moments published in the literature, as well as our new data, which were used for the analysis of (O−C) in this paper.

The first column L is the cycle number with respect to the epoch BJD 2449102.9200026 (the BJD of the first observation in Schwope et al. 1993). The $L = 0$ cycle here is shifted to epoch $T_0 =$ BJD 2453504.8882940 with constant offset of 50 702 cycles. The second column is the moment of the mid-egress in MJD. The third

Table A1. Mid-egress moments available in the literature.

Cycle L	MJD	Error (d)	Instrument	Ref.
0	49102.4200026	0.000 0029	*ROSAT*	1
1319	49216.9361120	0.000 0115	MCCP	2
1320	49217.0229220	0.000 0115	MCCP	2
1321	49217.1097490	0.000 0115	MCCP	2
1322	49217.1966010	0.000 0231	ESO1m	2
1333	49218.1516100	0.000 0231	ESO1m	2
1334	49218.2384390	0.000 0231	ESO1m	2
1367	49221.1035010	0.000 0231	ESO1m	2
1368	49221.1903190	0.000 0231	ESO1m	2
1369	49221.2771480	0.000 0231	ESO1m	2
2212	49294.4667944	0.000 0013	*ROSAT*	1
2213	49294.5536119	0.000 0031	*ROSAT*	1
2216	49294.8140780	0.000 0024	*ROSAT*	1
2222	49295.3349966	0.000 0024	*ROSAT*	1
2225	49295.5954591	0.000 0012	*ROSAT*	1
2226	49295.6822824	0.000 0018	*ROSAT*	1
4241	49470.6254248	0.000 0109	*ROSAT*	1
4409	49485.2112814	0.000 0276	*ROSAT*	1
6328	49651.8196284	0.000 0267	*ROSAT*	1
6341	49652.9483283	0.000 0066	*ROSAT*	1
6390	49657.2025335	0.000 0067	*ROSAT*	1
6391	49657.2893776	0.000 0200	*ROSAT*	1
6403	49658.3311948	0.000 0115	*ROSAT*	1
6576	49673.3511292	0.000 0134	*ROSAT*	1
6579	49673.6115921	0.000 0067	*ROSAT*	1
10707	50032.0062777	0.000 0246	*ROSAT*	1
12607	50196.9650434	0.000 0138	*ROSAT*	1
13064	50236.6420028	0.000 0104	*EUVE*	1
13620	50284.9141040	0.000 1157	AIP	2
13621	50285.0008780	0.000 1157	AIP	2
13632	50285.9558900	0.000 1157	AIP	2
13707	50292.4675175	0.000 0184	*EUVE*	1
14087	50325.4592540	0.000 0277	*HST*	2
14088	50325.5460740	0.000 0277	*HST*	2
14115	50327.8903240	0.000 1157	AIP	2
14116	50327.9771620	0.000 1157	AIP	2
14138	50329.8870410	0.000 1157	AIP	2
14139	50329.9738660	0.000 1157	AIP	2
14236	50338.3954800	0.000 0277	*HST*	2
14250	50339.6109856	0.000 0110	*EUVE*	1
14740	50382.1529766	0.000 0134	*ROSAT*	1
14746	50382.6739289	0.000 0187	*EUVE*	1
16906	50570.2059884	0.000 0067	*ROSAT*	1
17010	50579.2353441	0.000 0306	*ROSAT*	1
17030	50580.9717399	0.000 0095	*EUVE*	1
17994	50664.6666491	0.000 0203	*EUVE*	1
21014	50926.8642796	0.000 0134	*ROSAT*	1
21023	50927.6456491	0.000 0067	*ROSAT*	1
21026	50927.9061160	0.000 0067	*ROSAT*	1
22478	51053.9693474	0.000 0087	*EUVE*	1
22788	51080.8837110	0.000 1157	AIP	2
25892	51350.3743220	0.000 0115	OPT-ESO22	2
25926	51353.3262190	0.000 0115	OPT-ESO22	2
25938	51354.3680780	0.000 0115	OPT-ESO22	2
27394	51480.7786360	0.000 0231	AIP	2
29946	51702.3443352	0.000 0037	OPT-ESO22	4
29955	51703.1257050	0.000 0810	AIP	2
29955	51703.1257050	0.000 0925	CA123	2
29957	51703.2993545	0.000 0038	OPT-ESO22	4
29958	51703.3861705	0.000 0034	OPT-ESO22	4
29966	51704.0807040	0.000 0810	AIP	2
29966	51704.0807040	0.000 0925	CA123	2

Downloaded from http://mnras.oxfordjournals.org/ by guest on February 11, 2015

Table A1 – *continued*

cycle *L*	MJD	Error (d)	Instrument	Ref.
30265	51730.0400324	0.000 0041	OPT-SKO	4
30276	51730.9950648	0.000 0017	OPT-SKO	4
30277	51731.0818971	0.000 0019	OPT-SKO	4
30287	51731.9500901	0.000 0023	OPT-SKO	4
30299	51732.9919357	0.000 0033	OPT-SKO	4
30300	51733.0787554	0.000 0054	OPT-SKO	4
30310	51733.9469740	0.000 0031	OPT-SKO	4
30311	51734.0337856	0.000 0018	OPT-SKO	4
31312	51820.9410210	0.000 0115	STJ	2
31313	51821.0278410	0.000 0115	STJ	2
35043	52144.8679250	0.000 0463	AIP	2
35376	52173.7790965	0.000 0018	OPT-SKO	4
35377	52173.8659101	0.000 0022	OPT-SKO	4
35469	52181.8533851	0.000 0030	OPT-SKO	4
38098	52410.1041626	0.000 0084	OPT-SKO	4
38105	52410.7118710	0.000 0578	OM-UVM2	2
38107	52410.8855720	0.000 0231	XMM-MOS1	2
38107	52410.8855780	0.000 0231	XMM-MOS2	2
38108	52410.9723920	0.000 0231	XMM-PN	2
38109	52411.0591932	0.000 0034	OPT-SKO	4
38133	52413.1428510	0.000 0115	ULTRA-WHT	2
38145	52414.1847400	0.000 0115	ULTRA-WHT	2
39731	52551.8818440	0.000 0116	OPT-SKO	2
39742	52552.8368410	0.000 0116	OPT-SKO	2
42352	52779.4380340	0.000 0578	OM-UVM2	2
42395	52783.1712990	0.000 0115	ULTRA-WHT	2
42441	52787.1650399	0.000 0015	OPT-SAO	4
42463	52789.0750934	0.000 0014	OPT-SAO	4
42464	52789.1619272	0.000 0024	OPT-SAO	4
42486	52791.0719483	0.000 0015	OPT-SAO	4
42487	52791.1587715	0.000 0024	OPT-SAO	4
44534	52968.8800760	0.000 0033	OPT-NOT	4
44557	52970.8769377	0.000 0085	OPT-NOT	4
47253	53204.9447079	0.000 0027	OPT-SKO	4
47254	53205.0315288	0.000 0037	OPT-SKO	4
47300	53209.0252729	0.000 0038	OPT-SKO	4
47335	53212.0640023	0.000 0038	OPT-SKO	4
48265	53292.8069570	0.000 0102	OPT-SKO	4
48288	53294.8038228	0.000 0035	OPT-SKO	4
48299	53295.7588336	0.000 0066	OPT-SKO	4
48334	53298.7975567	0.000 0015	OPT-SKO	4
50702	53504.3882940	0.000 0056	ULTRA-VLT	2
50713	53505.3433170	0.000 0056	ULTRA-VLT	2
50714	53505.4301390	0.000 0056	ULTRA-VLT	2
50724	53506.2983420	0.000 0056	ULTRA-VLT	2
50725	53506.3851620	0.000 0056	ULTRA-VLT	2
50737	53507.4270080	0.000 0056	ULTRA-VLT	2
51020	53531.9971595	0.000 0100	OPT-SKO	4
51032	53533.0390170	0.000 0052	OPT-SKO	4
51066	53535.9909030	0.000 0064	OPT-SKO	4
51067	53536.0777278	0.000 0033	OPT-SKO	4
55466	53918.0007189	0.000 0046	OPT-SKO	4
55535	53923.9913426	0.000 0102	OPT-SKO	4
55546	53924.9463562	0.000 0075	OPT-SKO	4
55627	53931.9788164	0.000 0061	OPT-SKO	4
55661	53934.9307071	0.000 0064	OPT-SKO	4
55719	53939.9662754	0.000 0162	OPT-SKO	4
59524	54270.3179890	0.000 0157	ULTRA-VLT	2
59525	54270.4048120	0.000 0157	ULTRA-VLT	2
59558	54273.2698840	0.000 0157	ULTRA-VLT	2
59559	54273.3567040	0.000 0157	ULTRA-VLT	2

Table A1 – *continued*

Cycle *L*	MJD	Error (d)	Instrument	Ref.
60085	54319.0242409	0.000 0073	OPT-SKO	4
60096	54319.9792541	0.000 0037	OPT-SKO	4
60097	54320.0660769	0.000 0055	OPT-SKO	4
64657	54715.9671496	0.000 0053	OPT-SKO	4
64885	54735.7622085	0.000 0038	OPT-SKO	4
64886	54735.8490181	0.000 0016	OPT-SKO	4
65265	54768.7539926	0.000 0023	OPT-SKO	4
67604	54971.8267890	0.000 0390	YANO-24	3
67791	54988.0622710	0.000 0029	OPT-SKO	4
67917	54999.0016391	0.000 0017	OPT-SKO	4
67918	54999.0884526	0.000 0054	OPT-SKO	4
68009	55006.9891162	0.000 0017	OPT-SKO	4
68914	55085.5614770	0.000 0390	YANO-24	3
68926	55086.6033490	0.000 0390	YANO-24	3
69328	55121.5051450	0.000 0390	YANO-24	3
69490	55135.5700570	0.000 0390	YANO-24	3
69800	55162.4843420	0.000 0390	YANO-24	3
69812	55163.5261930	0.000 0390	YANO-24	3
69823	55164.4811950	0.000 0390	YANO-24	3
69915	55172.4686720	0.000 0390	YANO-24	3
71785	55334.8227620	0.000 0390	YANO-24	3
72009	55354.2706040	0.000 0004	NTT+UCAM	5
72010	55354.3574451	0.000 0005	NTT+UCAM	5
72099	55362.0844371	0.000 0032	OPT-SKO	4
72110	55363.0394546	0.000 0019	OPT-SKO	4
72121	55363.9944885	0.000 0029	OPT-SKO	4
72133	55365.0363444	0.000 0015	OPT-SKO	4
72225	55373.0238044	0.000 0048	OPT-SKO	4
72237	55374.0656456	0.000 0040	OPT-SKO	4
72248	55375.0206715	0.000 0040	OPT-SKO	4
72305	55379.9694292	0.000 0030	OPT-SKO	4
72351	55383.9631748	0.000 0024	OPT-SKO	4
72352	55384.0499944	0.000 0022	OPT-SKO	4
72421	55390.0406108	0.000 0013	OPT-SKO	4
73409	55475.8190971	0.000 0578	PIRATE	4
73559	55488.8421698	0.000 0578	PIRATE	4
73560	55488.9290151	0.000 1156	PIRATE	4
75467	55654.4954277	0.000 0040	MONET/N	4
75812	55684.4484608	0.000 0023	MONET/N	4
76053	55705.3721585	0.000 0009	NTT+UCAM	5
76348	55730.9841422	0.000 0054	OPT-SKO	6
76394	55734.9778822	0.000 0025	OPT-SKO	6
76395	55735.0646948	0.000 0023	OPT-SKO	6
76406	55736.0197228	0.000 0019	OPT-SKO	6
76464	55741.0552777	0.000 0093	OPT-SKO	6
76532	55746.9590878	0.000 0029	OPT-SKO	6
76555	55748.9559585	0.000 0017	OPT-SKO	6
76556	55749.0427747	0.000 0016	OPT-SKO	6
76567	55749.9978035	0.000 0019	OPT-SKO	6
76648	55757.0302482	0.000 0071	OPT-SKO	6
76721	55763.3681410	0.000 0035	MONET/N	4
76868	55776.1307426	0.000 0020	LT+RISE	5
77031	55790.2824571	0.000 0039	MONET/N	4
77066	55793.3211556	0.000 0077	MONET/N	4
77067	55793.4079841	0.000 0055	MONET/N	4
77078	55794.3630179	0.000 0065	MONET/N	4
77247	55809.0356564	0.000 0025	LT+RISE	5
77546	55834.9949490	0.000 0179	WFC	4
77557	55835.9499905	0.000 0295	WFC	4
77789	55856.0922852	0.000 0038	MONET/N	4
77802	55857.2209399	0.000 0090	MONET/N	4
77823	55859.0441786	0.000 0066	MONET/N	4

Downloaded from http://mnras.oxfordjournals.org/ by guest on February 11, 2015

Table A1 – *continued*

cycle L	MJD	Error (d)	Instrument	Ref.
77902	55865.9029864	0.000 0022	LT+RISE	5
78100	55883.0934038	0.000 0022	MONET/N	4
80324	56076.1818394	0.000 0022	LT+RISE	5
80485	56090.1598976	0.000 0019	LT+RISE	5
81001	56134.9591635	0.000 0071	OPT-SKO	6
81013	56136.0010300	0.000 0058	OPT-SKO	6
81162	56148.9372694	0.000 0059	OPT-SKO	6
81186	56151.0209490	0.000 0020	OPT-SKO	6
81231	56154.9278501	0.000 0034	OPT-SKO	6
81486	56177.5670248	0.000 0008	WHT+UCAM	5
81531	56180.9739470	0.000 0022	LT+RISE	5
81532	56181.0607721	0.000 0006	WHT+UCAM	5
81910	56213.8788462	0.000 0002	WHT+UCAM	5
82566	56270.8329602	0.000 0053	LT+RISE	5
84275	56419.2088830	0.000 0011	LT+RISE	5
84678	56454.1974374	0.000 0017	LT+RISE	5
85746	56546.9214776	0.000 0073	PIVA-NAO	6
85965	56565.9351702	0.000 0010	LT+RISE	5
86032	56571.7520793	0.000 0034	PIVA-NAO	6
86391	56602.9205819	0.000 0016	LT+RISE	5
86412	56604.7437774	0.000 0027	PIVA-NAO	6
86433	56606.5670216	0.000 0045	TNT+USPEC	5
86467	56609.5189097	0.000 0021	TNT+USPEC	5
86976	56653.7104280	0.000 0361	PW24-COG	6
88383	56775.8665044	0.000 0017	ULTRA-TNT	6
88973	56827.0904134	0.000 0016	INT+WFC	5
88985	56828.5322517	0.000 0037	INT+WFC	5
89066	56835.1647131	0.000 0024	LT+RISE	5
89339	56858.8666325	0.000 0064	PIVA-NAO	6
89340	56858.9534517	0.000 0103	PIVA-NAO	6

column is the quoted mid-egress error in the relevant source publication, derived on the basis of observations with 'Instrument' (fourth column). Instruments are code-named in accord with a particular source publication: '1' is for Schwope et al. (2001), '2' is for Schwarz et al. (2009), '3' is for Qian et al. (2011), '4' is for Goździewski et al. (2012), '5' is for Bours et al. (2014) and '6' is for this work. The mid-egress measurements in Qian et al. (2011) are included in Table A1; however, these data were not used for constraining our models, since they differ by ∼10 s from accurate OPTIMA and MONET/N points, spanning the same observational window Goździewski et al. (2012). There are 215 data mid-egress JD measurements in total, but only $N_{\rm obs} = 205$ points were used in this paper.

This paper has been typeset from a TEX/LATEX file prepared by the author.

Downloaded from http://mnras.oxfordjournals.org/ by guest on February 11, 2015